Osmotic dehydration of replacement lung surfactant: Implications for ARDS therapy

by

An Thien Ngo

A.B., Bryn Mawr College, 2002

Submitted to the Graduate Faculty of

Arts and Sciences in partial fulfillment

of the requirements for the degree of

Master of Science

University of Pittsburgh

2004

UNIVERSITY OF PITTSBURGH

FACULTY OF ARTS AND SCIENCES

This dissertation was presented

by

An Thien Ngo

It was defended on

December 16, 2004

and approved by

Dr. Gilbert C. Walker

Dr. Stephen G. Weber

Dr. David H. Waldeck
Dissertation Director

Osmotic dehydration of replacement lung surfactant:
Implications for ARDS therapy

An Thien Ngo, M.S.

University of Pittsburgh, 2004

The potentially fatal condition of Acute Respiratory Distress Syndrome (ARDS) begins with damage to the lung, which then becomes flooded with fluid rich in serum protein. These serum proteins inactivate the lung surfactant (LS) that lines the alveoli, raising alveolar surface tension and resulting in lung collapse. Previous studies have shown that the addition of nonionic polymers to therapeutic replacement lung surfactant (RLS) restores the surface activity of RLS in the presence of inactivating substances, a possible explanation being the dehydration of RLS vesicles by polymer-induced depletion forces. This study tested the hypothesis that RLS whose surface activity responds to the addition of polymer will also experience dehydration upon application of known osmotic stress.

The interlamellar spacing *d* of the porcine extract RLS Curosurf and the synthetic RLS Exosurf was measured using small-angle X-ray scattering in the presence of polymer and/or bovine serum albumin (BSA) at various concentrations. The applied osmotic pressures were 10^0 – 10^8 dynes/cm^2. Over this range of pressures, Curosurf experiences a 50Å change in *d* that fits an exponential curve with decay constant of 7.22 ± 0.23 Å, similar to the Debye length in 150 mM solution. This may indicate the presence of electrostatic interactions. The Exosurf *d* lie within a range of 59-72 Å but exhibit no definite trend. These results suggest that added polymer in the concentrations utilized would not improve the surface activity of Exosurf, but that osmotic stress may indeed be a mechanism by which polymers restore the function of inactivated Curosurf. Polymers used were polyethylene glycol (PEG, 10 or 20 kDa) and 150 kDa Dextran.

To investigate the effect of PEG on the surface activity of Exosurf, pressure-area isotherms of Exosurf spread from chloroform on 150 mM NaCl, 5 mM CaCl2, 1.5 mM tris-HCl, pH 7.2-7.4, were recorded at 24.5ºC in the presence and absence of 5% PEG (m.w. 10 kDa) and 2 mg/mL BSA. Upon repeated compressions of Exosurf on 5% PEG solution, a decrease in the length of the fluid-condensed phase coexistence region in the isotherm suggested the dissolution of Tyloxapol into the subphase.

TABLE OF CONTENTS

LIST OF TABLES

LIST OF FIGURES

ACKNOWLEDGEMENTS

Dr. Heidi Warriner (Raytheon Company, California), my primary advisor on this project. During her assistant professorship at the University of Pittsburgh, she introduced me to the fields of biological lipid membranes and small-angle X-ray diffraction. The short courses and internships that she encouraged me to attend have enriched my education. I especially appreciate her feedback on my written document and presentation.

Dr. Darryl Sasaki (Sandia National Laboratories, New Mexico)*. Dr. Sasaki sponsored my visit to Sandia in 2004, where I carried out the Langmuir trough experiments for this project. Sandia researchers Jaclyn Murton, Jenny Pincus, and Dr. Andrea Slade introduced me to new methods in the study of monolayers and vesicles.

Dr. Junqi Ding (Unilever Research U.S., New Jersey / Connecticut), who invited me to work at Unilever while I wrote up my thesis. Dr. Ding also provided input on Langmuir trough design, and feedback on my document.

Dr. Joseph Zasadzinski (University of California- Santa Barbara). In his laboratory I started research with Dr. Warriner during her postdoctoral fellowship in the summer of 2002. I appreciate his hospitality, and the departmental funding from Pitt, that gave me this opportunity.

Gary Ganley (Bruker-AXS) set up the SAXS diffractometer and provided training.

I would also like to thank the following people from the University of Pittsburgh:

- Evon Nigro, Toni Weber, and Fran Nagy skillfully coordinated my travel.
- Roy Watters and Robert Muha built the components and thermistor circuit for a homemade Langmuir trough not otherwise mentioned in this thesis.
- My undergraduate research advisors: Dr. Xiao-Lun Wu and Dr. Eric Borguet.
- My colleagues in Dr. Warriner's laboratory: Daniel Lamont, Oleg Golik, and Scott Quivey.
- Trustees of the Mary E. Warga Predoctoral Fellowship and the Ashe Fellowship.

Finally, I thank my mom, dad, and sister Tam for their many years of love and support.

*Sandia is a multiprogram laboratory operated by Sandia Corporation, a Lockheed Martin Company for the United States Department of Energy's National Nuclear Security Administration under contract DE-AC04-94AL85000

Dedicated to

Professor Julia Ann Thompson
(March 13, 1943 – August 16, 2004)

Her friendship was a priceless gift.

1. INTRODUCTION

The lipids and proteins which comprise natural lung surfactant (LS) are secreted by the alveolar type II cells of the lung, and exist in the fluid lining of the alveoli as lamellar aggregates, vesicles, tubular myelin structures, and a monolayer at the air-water interface[1]**.** The monolayer undergoes reversible phase transitions as the area available to it changes during breathing. Its primary function is to reduce surface tension in an area-dependent fashion so that the surface tension is near zero when the alveoli are smallest. The relationship between low surface tension and lung surfactant function is described in **Section 2.1.1**. NRDS (neonatal respiratory distress syndrome) results from LS deficiency. Elevated alveolar surface tensions cause lung collapse, reducing lung volume, injuring lung tissue, and decreasing blood oxygenation [2]. ARDS (acute respiratory distress syndrome) shares many symptoms with NRDS, but stems from surfactant inactivation rather than surfactant deficiency and can furthermore occur at all ages; NRDS is limited to infants born before LS production begins.

ARDS is a vicious cycle that begins with damage to the lung, which then becomes flooded with fluid rich in serum protein. These serum proteins inactivate the surfactant lining the alveoli. Lung collapse can result from increased surface tension within the alveoli; the subsequent stretching of surfactant-deficient alveolar structures produces further damage [3]. In 50% of patients, respiratory distress develops within 24 hours of the initial insult [4], which provides a window of opportunity for prophylactic treatment. Though the body's repair of lung tissue begins within 7 to 28 days, lasting respiratory impairment is common, and the healing process may continue for up to 12 months [5]. An NIH study in 1972 found 150,000 cases of ARDS per year [6]; this has been widely cited but may be an overestimate [4]. Physical trauma and aspiration of gastric contents are common initiators of ARDS [4].

Table 1 describes the composition of three commercially available replacement lung surfactants (RLS): Exosurf, Curosurf, and Survanta. Curosurf is an organic extract of minced porcine lungs, suspended in 150 mM NaCl. Its primary components are phosphatidylcholine, phosphatidylethanolamine, and sphingomyelin, which are all neutral phospholipids; it also contains a total of 6 % charged lipids. Survanta is an organic extract of minced bovine lung, to which dipalmitoylphosphatidylcholine (DPPC), palmitic acid (PA), and tripalmitin have been added. Both Survanta and Curosurf also contain a small amount of surfactant proteins SP-B and

SP-C. Exosurf is a completely synthetic, protein-free RLS whose possible advantages include low cost and well-defined composition [7]. However, it is less effective than Curosurf or Survanta in the treatment of NRDS [8]. 6% of its composition is a non-biological surfactant (Tyloxapol).

Name	**Source (animal/synthetic)**	**Composition**	**Manufacturer**
Exosurf	Synthetic in 100 mM NaCl	85 % DPPC 9% hexadecanol 6% tyloxapol [9,10]	GlaxoSmithKline, USA
Curosurf	Minced porcine lung extract in 150 mM NaCl	99 % phospholipid 1% surfactant protein (SP-B, SP-C) Phospholipid Content: ~64% PC, ~12% PE, ~10% SPH, ~2% each of PI/PG/PS [11]	Chiesi Farmaceutici, Italy
Survanta	Minced bovine lung extract, + DPPC, PA and tripalmitin; cholesterol removed in 150 mM NaCl	25 mg/mL phospholipids, incl. 11.0-15.5 mg/mL DPPC 0.5-1.75 mg/mL triglycerides, > 1 mg/mL SP-B, SP-C [7]	Abbott Laboratories, USA

Table 1. Some replacement lung surfactant compositions. DPPC: dipalmitoylphosphatidylcholine. PC: phosphatidylcholine. PE: phosphatidylethanolamine. SPH: sphingomyelin. PI: phosphatidylinositol. PG: phosphatidylglycerol. PS: phosphatidylserine.

While RLS therapy has dramatically reduced mortality in NRDS, the inactivation of RLS by serum proteins, meconium (neonatal feces) and other substances has hindered the use of RLS therapy for ARDS patients. The development of an inactivation-resistant RLS is thus a desirable goal [12]. Taeusch[13] and Kobayashi[14], working independently of each other, demonstrated that addition of nonionic polymers such as polyethylene glycol or dextran permits RLS to maintain low surface tensions and rapid adsorption rates even in the presence of substances known to inactivate LS. These groups modeled the alveolus using a modified pulsating bubble surfactometer [15], which consists of a chamber filled with surfactant solution into which a bubble is introduced via an air-filled dry capillary. Pressures applied to this solution via a piston cause the bubble to shrink or expand, mimicking the deflation and inflation of an alveolus during breathing. Surface tension is determined using the Young-Laplace equation (**Equation 1**) and the bubble's radius.

Selected findings from Taeusch are plotted in **Figure 1** for mixtures of Survanta, Curosurf, and various polymers in the presence and absence of meconium, which is fecal matter sometimes inhaled by infants during birth. The polymers utilized were polyethylene glycol, dextran (a glucose polymer), and polyvinylpyrrolidone. Minimum surface tension (γ_{min}) was measured after the tenth deflation in the pulsating bubble surfactometer described above. While the γ_{min} of unadulterated Survanta rises from approximately 3 mN/m to 30 mN/m at 3% meconium, the γ_{min} of the Survanta – polymer mixtures remains near zero at all meconium concentrations. This is comparable to the behavior of whole dog surfactant, and an improvement over a mixture of Survanta and surfactant protein A (SP-A), a glycoprotein abundant in natural lung surfactant. **Figure 2** shows complementary results from Tashiro and coworkers [16], who found that addition of dextran lowered the γ_{min} of a Curosurf mixture to which 5 mg/mL meconium had been added. The minimum surface tension of the mixture fell from approximately 22 mN/m (unadulterated Curosurf plus meconium) to about 2 mN/m with the addition of 10 mg/mL dextran.

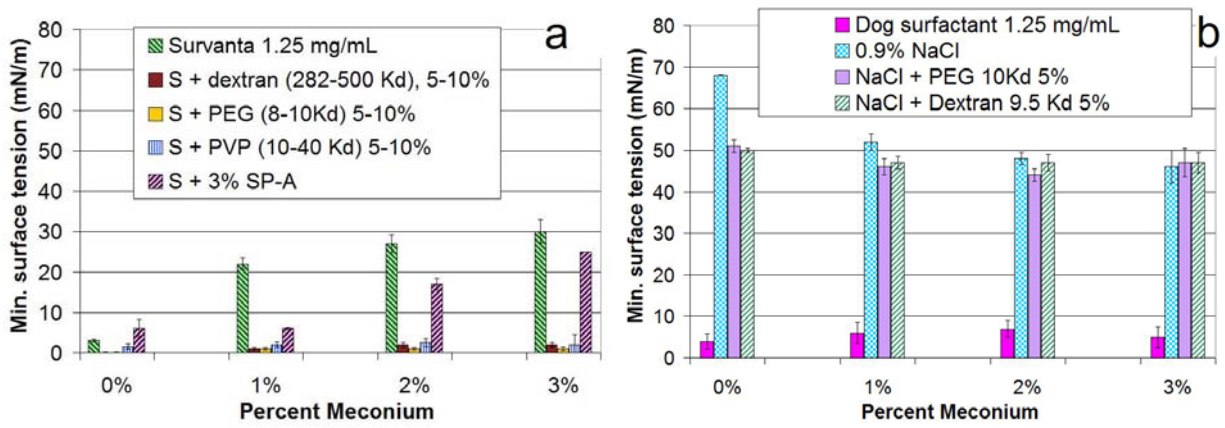

Figure 1 . Minimum surface tension after tenth bubble deflation in a pulsating bubble surfactometer, in the presence or absence of meconium. Solvent is 0.9% NaCl, 5mM HEPES, pH 7.0-7.2, at 37ºC. Data is re-plotted from Taeusch et al, *AJRCCM* 1999.
(a) Mixtures of Survanta (1.25 mg/mL) with polymer or surfactant protein A.
(b) Whole dog surfactant, or mixtures of buffer with polymer.

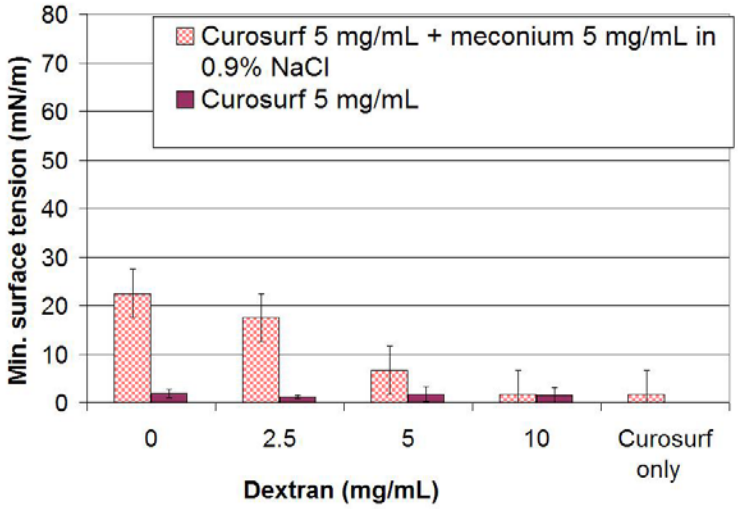

Figure 2. Effect of meconium and dextran on the minimum surface tension of Curosurf, measured with a pulsating bubble surfactometer. Data is re-plotted from Tashiro et al, *Acta Paediatr* 2000.

While polymer interactions with lipid membranes have been extensively characterized [17-19] [20] [21], their application to multicomponent aggregates of lung surfactant was first proposed by Taeusch [13], who suggested that the behavior of LS-polymer mixtures may be related to polymer exclusion from lipid vesicles. The resulting osmotic stress may have ramifications for a variety of surfactant characteristics, including adsorption rate and concentration of surface-associated lipids [12].

We wish to directly determine if and how osmotic stress affects RLS whose surface activity responds to the addition of polymer. The interactions between hydrophilic polymers and lipid membranes may include polymer exclusion from the membrane surface, with a resulting depletion attraction [22], but could also involve repulsive forces if the polymer were to adsorb onto the membranes [23]. If the polymer is neither attracted to nor repelled from the membrane surface, no forces will be exerted by it, and the above mechanisms can be eliminated from the possible modes of polymer-vesicle interaction.

Our data shows that Curosurf, a porcine extract surfactant for which the interfacial effects of polymer include decreased adsorption time and lower minimum surface tension [16], exhibits a reduction in interlamellar spacing upon application of $10^0 - 10^8$ dyne/cm^2 osmotic pressure. This indicates that osmotic stress does draw water out of Curosurf vesicles and may contribute to Curosurf's improved surface activity upon the addition of polymer. Exosurf, a protein-free synthetic surfactant, exhibits no definite trend; the data is distributed over a 10Å range that does not appear to depend on the exerted pressures. We therefore predict that polymer addition will not improve Exosurf's ability to lower surface tension in the presence of substances known to inactivate LS.

2. BACKGROUND

2.1.Biological function of lung surfactant

An effective lung surfactant must be able to:

(1) reach a minimum surface tension γ_{min} near zero mN/m at small alveolar surface areas upon dynamic compression.

(2) exhibit an equilibrium surface tension (γ_{eq}) of 25 mN/m

(3) adsorb rapidly to coat the entire alveolar interface

The definition of, and rationale for, each of these criteria is described below.

2.1.1. Minimum surface tension of zero upon dynamic compression

The minimum surface tension, γ_{min} , is a non-equilibrium property obtained by reducing the amount of surface area available to the surfactant monolayer, so that the concentration of molecules at the interface is greater than at equilibrium The surface tension γ_{min} is thus lower than the equilibrium surface tension $\gamma_{eq.}$

The lung contains over 300 million alveoli, lined with surfactant-containing fluid and possessing a total internal surface area of about 70 m^2. Inflation of the lung is achieved by contraction of the diaphragm, which expands the volume of the thoracic cavity. This decreases the pressure within the alveoli; air thus flows into the lung. The reduction in surface tension due to the action of lung surfactant is essential to this process [2].

A spherical fluid cavity with radius of curvature *R* requires an inflation pressure ΔP that is related to the fluid's surface tension by the Young-Laplace equation [24].

$$\Delta P = \frac{2\gamma}{R}$$

Equation 1. The Young-Laplace equation for a spherical curved surface.

The alveoli can be represented as connected cavities in the alveolar fluid. On average, each alveolus has radius 0.05 mm at rest and 0.1 mm when inflated. In premature infants lacking surfactant, the alveolar fluid has the surface tension of water, approximately 70 millinewtons per meter at 37ºC. Under these conditions, a deflated alveolus would need to contain 21.7 mm Hg

greater pressure than atmospheric (the pressure within the thoracic cavity surrounding the alveoli) to maintain its radius of 0.05 mm. An inflated alveolus would require +10.9 mm Hg to maintain its radius of 0.10 mm. The decrease in pressure compared to the deflated alveolus would drive the flow of air into the lung.

$$\Delta P_{def} = \frac{2\gamma}{r} = \frac{2(70 dyne/cm)}{0.005 cm} = 28000 dyne/cm^2 \left(\frac{0.000015 psi}{dyne/cm^2}\right)\left(\frac{760 mmHg}{14.696 psi}\right) = 21.7 mmHg$$

$$\Delta P_{\inf} = \frac{2\gamma}{r} = \frac{2(70 dyne/cm)}{0.01 cm} = 14000 dyne/cm^2 \left(\frac{0.000015 psi}{dyne/cm^2}\right)\left(\frac{760 mmHg}{14.696 psi}\right) = 10.9 mmHg$$

However, at rest ΔP_{def} is zero; the alveoli contain atmospheric pressure. The expansion of the thoracic cavity only reduces the internal alveolar pressure by 1-2 mm Hg. Surface tension must therefore be reduced to zero in order for the alveoli to remain inflated at rest, and to inflate with such a small pressure decrease. [2]

2.1.2. Reach equilibrium surface tension of 25 mN/m

γ_{eq} is related to bulk concentration by the Gibbs surface excess Γ_2^1, which is the excess amount of solute adsorbed per unit surface area of a liquid[25,26]. The extent of solute adsorption can be calculated from the Gibbs adsorption equation using data on the change in γ_{eq} with molar or molal solute concentration c_2.

$$\Gamma_2^1 = -\frac{1}{RT}\left(\frac{d\gamma}{d\ln c_2}\right)$$

Equation 2. The Gibbs adsorption equation.

A 5 mg/mL solution of natural LS in 0.15 mM NaCl and 5 mM $CaCl_2$, extracted by saline lavage of calf lungs, reaches γ_{eq} of 25 mN/m after 10 s of adsorption in a pulsating bubble apparatus. Calf lung extract surfactant (CLSE), obtained by chloroform:methanol extraction, also reaches γ_{eq} of 25 mN/m under the same conditions [27]. An RLS that most closely approximates the behavior of natural LS must therefore exhibit similar γ_{eq}.

2.1.3. Adsorb rapidly to coat the interface

Lipid aggregates closely associated with the interface are said to play an important role in adsorption. For example, small vesicles of DPPC adsorb more rapidly and lower surface tension more effectively than large liposomes [28]. Surfactant subtypes of different morphologies, varying in concentration of surfactant protein, exhibit different surface activities though their phospholipid content is identical [1]. A more detailed explanation of the relationship between aggregate structure and adsorption is given in the "Lipid Mechanics" section of this paper. Here, characteristics of adsorption relevant to lung surfactant are described.

During inhalation to total lung capacity (TLC), it is necessary that surfactant adsorb rapidly so that low surface tensions can be maintained and a single breath is sufficient to bring new surfactant to the interface. [29]. Surfactant concentration and composition both govern adsorption rate; for example, a 1 mg/mL suspension of bovine lipid extract surfactant (bLES) reaches a γ_{eq} of 25 mN/m in just 5 seconds, while a 200 microgram-mL suspension of the same surfactant requires over 30 seconds to reach the same surface tension [30]. In contrast, a 100 microgram/mL suspension of Exosurf reaches a γ_{eq} of 34.5 ± 0.5 mN/m in 15 minutes, indicating that Exosurf may perform poorly as a replacement lung surfactant compared to bLES.

Rapid adsorption appears to take place incrementally, where surface tension decreases with step sizes ranging from 1 to 10 mN/m. These adsorption "clicks", so named because they cause a captive bubble to suddenly change height in a clicking fashion, are ascribed to aggregates containing approximately 10^{14} molecules of DPPC and 10^{11} molecules of surfactant proteins (a mixture of SP-B and SP-C) [29]

Adsorption to γ_{eq} yields a reservoir of surfactant aggregates remaining closely associated with the surface monolayer. Schurch [29] demonstrated this by introducing an air bubble into a solution of Curosurf, allowing the surfactant to adsorb, then carefully replacing all of the bulk solution with surfactant-free saline. The bubble was then expanded by moving a piston that increased the sample chamber volume. Expanding the bubble past its original size should have increased the surface tension above the equilibrium value if the surfactant had only formed a monolayer; however, the observed plateau in surface tension indicated that excess material had also been associated with the interface. Continuing to compress the surface film past the point of γ_{min} yields a collapse phase in addition to this reservoir [30].

2.2.Inhibition of replacement lung surfactant

While the fibrin monomer is the most potent inhibitor of lung surfactant (LS), albumin comprises a larger fraction of the total serum proteins [31] and is therefore the inhibitor of interest in this paper. Previous studies have concluded that albumin inactivates LS by competition for the interface[27,32,33]. Warriner and coworkers furthermore found that albumin inserts into model LS monolayers at a surface pressure equal to the surface pressure of the bulk albumin solution[34]. When the albumin concentration was changed, so did the bulk solution surface pressure and therefore the insertion pressure. The albumin at the surface reduced the area available to the LS molecules, preventing respreading of collapsed material. Since the collapsed LS could not respread to coat the surface, lower surface pressures prevailed upon subsequent compressions of the monolayer.

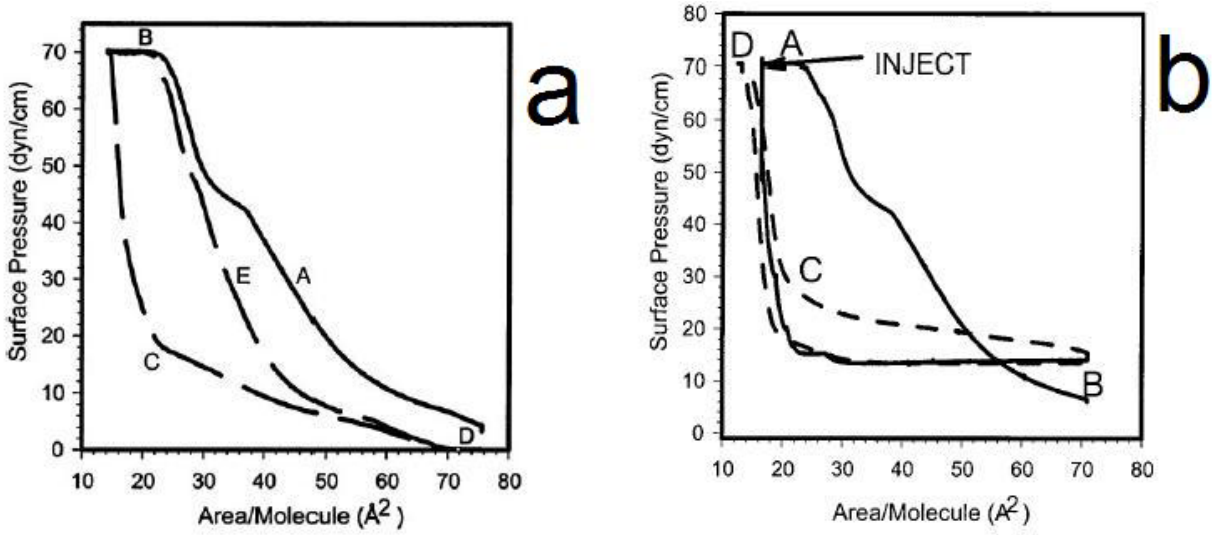

Figure 3. Relationship between inhibition and equilibrium spreading pressure. (a) 69/21/10 wt% DPPC/POPG/PA on 25 °C 150 mM NaCl, 2 mM CaCl2, 0.2 mM NaHCO3 , pH 7, 0.5-1 mol% TR-DHPE added for imaging. (b) Same composition as (a). Compressed to A. BSA injected to a final concentration of 2 mg/mL and allowed to equilibrate. Re-expanded to B, then compressed to C and D. Reprinted with permission from Warriner et al, *Biophys. J.* 2002. Copyright (2002) Biophysical Society.

2.3. Osmotic stress

A non-adsorbing solute draws water from lipid vesicles by initiating a gradient in the chemical potential of water. The gradient can be viewed as work (w) done by osmotic pressure P_{osm} on a volume of water dV located between or within vesicles.

$$w = -P_{osm} dV$$

Equation 3. Osmotic pressure does work by changing the volume of water between or within vesicles.

This can induce aggregation of vesicles surrounded by a depletion layer in polymer solution; or reduction in the interlamellar spacing of vesicles where the solute concentration outside the vesicles differs from that within them (**Figure 4)**. The latter situation is considered in this paper; both cases are based on thermodynamic concepts summarized by Parsegian [19].

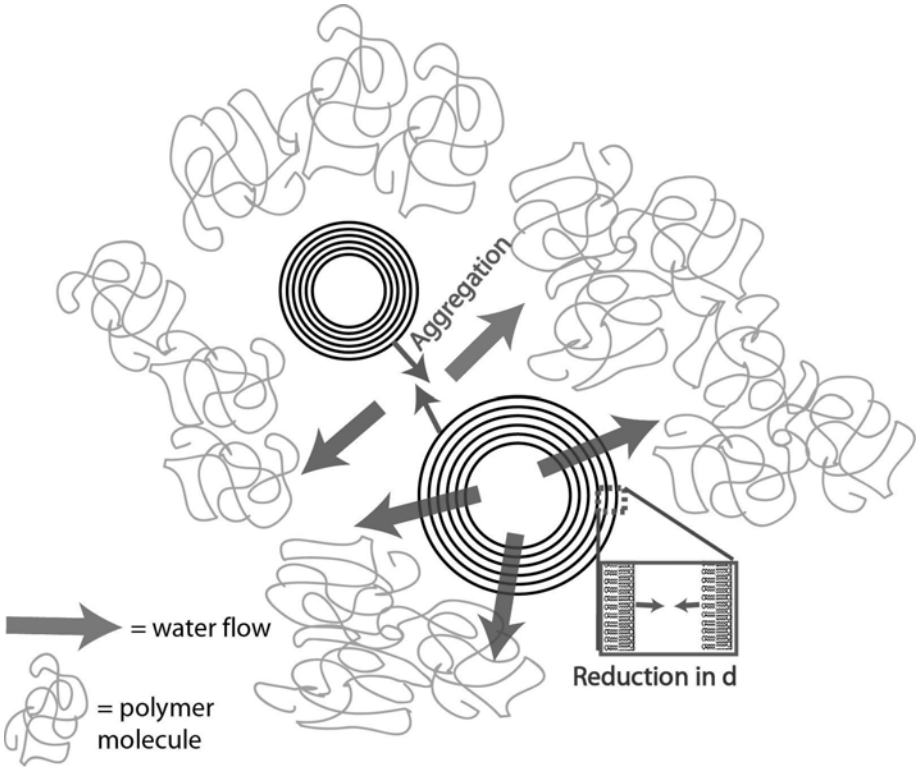

Figure 4. Osmotic stress can induce aggregation or reduction in d-spacing of multilamellar vesicles.

For a solute to exert osmotic stress, its concentration adjacent to the vesicles must differ from that in the bulk [19]. This in turn changes the water concentration, which is related to the water's chemical potential.

The chemical potential of a solute x depends on its concentration C_x, as well as the solute-solvent interactions and the temperature. This is shown in **Equation 4**, where σ is the solute activity coefficient[1], T is temperature (Kelvin), and k is Boltzmann's constant (1.38 x 10^{-23} J/K).

$$\mu_x = kT\ln(\sigma C_x)$$

Equation 4. Dependence of chemical potential on concentration.

Both vesicular aggregation and movement of lamellae involve movement of mass, which flows according to gradients in chemical potential. The chemical potential of each component in a solution can affect that of other components.

Consider a quantity N_M of multilamellar vesicles M in a solution of water (w) containing a solute (s). The number of water molecules around the vesicles is N_w and the number of solute molecules is N_s. The Gibbs-Duhem equation describes the constraints on the free energy of the system; namely, that no net effect should result from changes in free energy induced by altering the temperature (T), pressure (P), and chemical potential (μ).

$$0 = SdT - VdP + (N_M d\mu_M + N_s d\mu_s + N_w d\mu_w)$$

Equation 5. Gibbs-Duhem equation for a multilamellar vesicle *M* in a solution of water (*w*) and solute (*s*).

For N_M = 1 at constant temperature and pressure, this equation can be rewritten so that changes in the vesicle's chemical potential $d\mu_M$ depend only on changes in the solute and water chemical potentials $d\mu_s$ and $d\mu_w$.

$$d\mu_M = -(N_s d\mu_s + N_w d\mu_w)$$

Equation 6. Relationship between chemical potentials of components in a solution at constant T and P.

[1]Though the activity coefficient is often denoted by γ, it is represented by σ here to avoid confusion with the notation employed for surface tension.

A vesicle-free reference solution can also be defined, where the water and solute quantities are represented by n_w and n_s. These quantities can refer to the environment within the vesicle, or concentrations in bulk solution far from the vesicle. At constant temperature and pressure, $d\mu_s$ and $d\mu_w$ can be written in terms of each other via the Gibbs-Duhem equation.

$$0 = \left(n_s d\mu_s + n_w d\mu_w\right)$$
$$d\mu_s = -\frac{n_w}{n_s} d\mu_w$$
$$d\mu_w = -\frac{n_s}{n_w} d\mu_s$$

Equation 7. Chemical potentials of water and solute in a vesicle-free solution at constant T and P.

Replacing $d\mu_w$ in **Equation 6** with its definition in **Equation 7** yields an expression where the change in vesicular chemical potential $d\mu_M$ depends on the bulk concentrations n_s and n_w. as well as $d\mu_s$, N_s and N_w . Rearrangement of this expression reveals that the ratios N_s / N_w and n_s / n_w must differ in order for $d\mu_M$ to be nonzero. The dependence of $d\mu_M$ on $d\mu_w$ can be derived in a similar fashion.

$$d\mu_M = -\left(N_s d\mu_s - N_w \frac{n_s}{n_w} d\mu_s \right)$$
$$d\mu_M = -N_s \left(1 - \frac{N_w}{N_s} \frac{n_s}{n_w} \right) d\mu_s$$

or

$$d\mu_M = -\left(N_s \frac{n_w}{n_s} d\mu_s - N_w d\mu_s \right)$$
$$d\mu_M = -N_w \left(1 - \frac{N_s}{N_w} \frac{n_w}{n_s} \right) d\mu_w$$

Equation 8. The relationship between solute, water, and vesicular chemical potentials depends on the differences in concentration around the vesicle.

An example of the dehydration of lipid vesicles by osmotic stress is shown in **Figure 5**, where the chemical potential of water in a vesicular solution was altered using a variety of methods that exerted different amounts of osmotic pressure. The lowest-pressure method ($P \leq 10$ atm) involved placing the solution in equilibrium with a polymer solution through a dialysis membrane. Higher pressures were applied by piston, where water escaped through a membrane (6 atm = P = 500 atm), and by equilibration with saturated salt solution whose partial pressure of water in the vapor phase was lower than the vapor pressure of pure water (225 atm $\leq P \leq$1500 atm). The lipids were a mixture of phosphatidylcholines obtained from chicken eggs, with an average molecular weight of 790. An exponential decrease in *d* with pressure was observed, which corresponded to removal of water from the interlamellar space. The data are replotted in **Figure 5,** with $\log_{10}P$ on the y-axis and *d* (Å) on the x-axis.

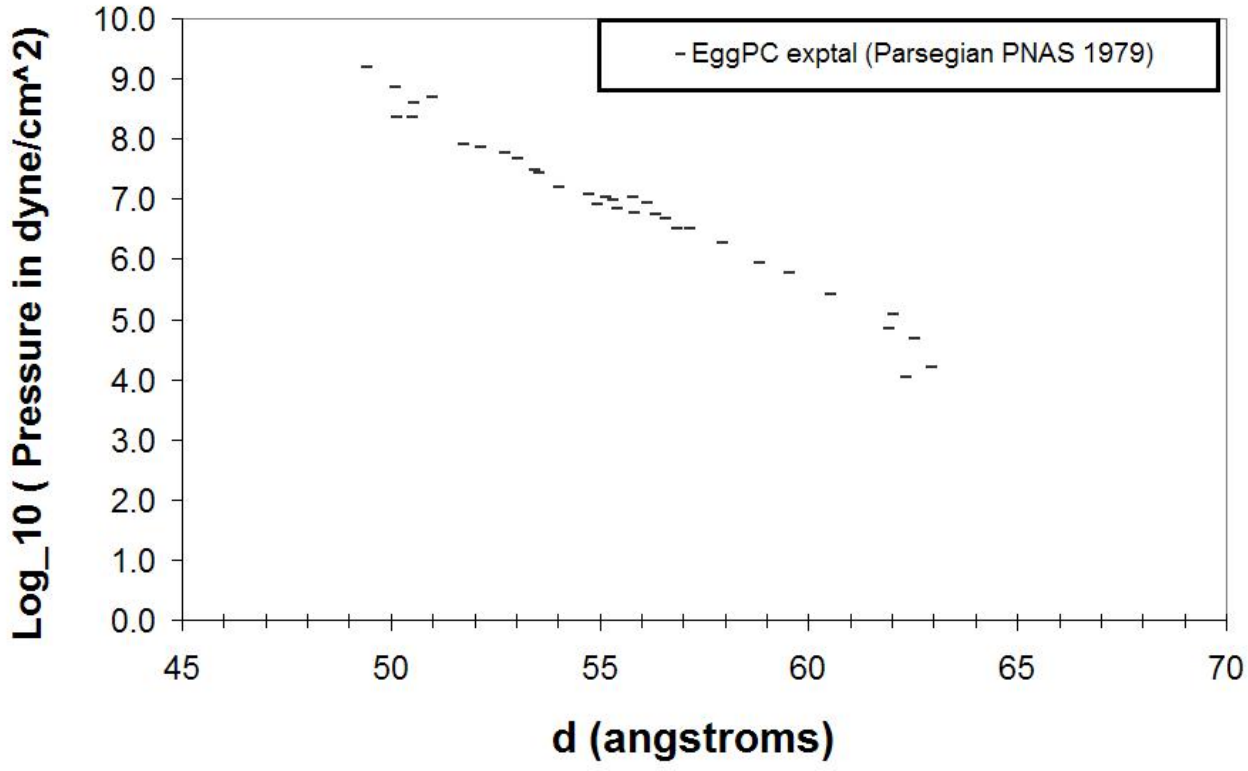

Figure 5. Dehydration of mixed phosphatidylcholine vesicles by osmotic pressure. Data are replotted from Parsegian et al, *PNAS* 1979.

2.4.Lipid mechanics

Liposomes consist of lipid bilayers surrounding an aqueous solution, and can be classified into at least three categories: multilamellar vesicles (MLV), small unilamellar vesicles (SUV) and large unilamellar vesicles (LUV). Molecular geometry determines whether a mixture of lipids will form a vesicle at all [35], while the preparation method can determine whether the mixture forms MLVs, SUVs, or LUVs. MLVs can be prepared by evaporating the solvent from an organic solution of lipids and hydrating the resulting thin lipid film with buffer above the transition temperature of the highest-melting component[36], which is the method utilized to prepare vesicles of Exosurf in the present study.

Osmotic removal of water from vesicles causes them to decrease in radius and thus increase in curvature. The distance d_w between lamellae also decreases. Though osmotic stress is capable of changing the headgroup area or bilayer thickness d_L [17] [20], we assume that these dimensions remain constant over the range of applied pressures. This assumption is borne out by our observation of the exponential decrease in Curosurf d-spacing with applied pressure; a change in d_L would have required that some of the applied pressure go into inducing this phase transition, which would have disrupted the linear relationship of d with $\log_{10}P$.

Deformation increases the interfacial free energy of the bilayer, favoring vesicle rupture or fusion with flat interfaces [37]. This phenomenon is the basis for our hypothesis regarding the mechanism by which PEG helps lung surfactant maintain low surface tensions.

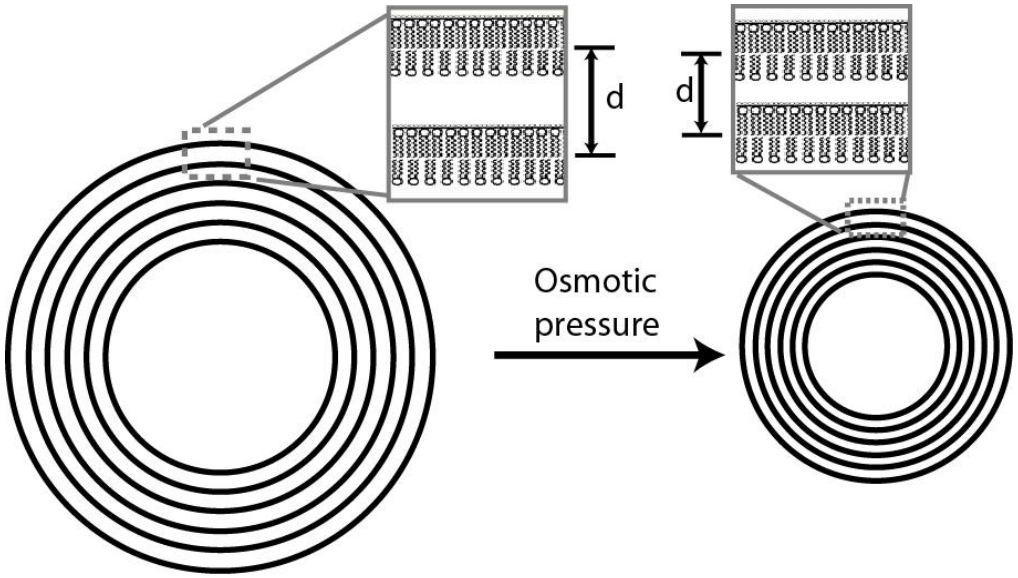

Figure 6. Vesicular shrinkage, and the resulting increase in curvature, upon applied osmotic stress.

2.4.1. Curvature dependence of interfacial free energy

Self-assembly arises from the balance of attractive and repulsive forces between amphiphilic molecules. These interactions can include hydrophobic attractions, depletion attractions, steric repulsions, or electrostatic interactions. The interaction free energy per molecule in a bilayer vesicle containing N molecules is given by

$$\mu_N^o = 2\gamma a_o + \frac{\gamma}{a}(a - a_o)^2 + \frac{k_b}{2}\left(\frac{1}{R^2} - \frac{1}{R_c^2}\right)$$

Equation 9. Interaction free energy per molecule in a bilayer vesicle.

where the optimal headgroup area a_o and the critical vesicle radius R_c are characteristic of the molecule, being based on molecular geometry, while the actual radius R and headgroup area a represent features of the specific vesicle. The interfacial energy per molecule γ is calculated at the hydrocarbon-water interface, that is, the boundary between the hydrocarbon tails and hydrophilic headgroups of the molecules in the bilayer. The bending modulus k_b, on the other hand, accounts for repulsions taking place some distance away from this boundary, normal to the bilayer. This is illustrated in **Figure 7**. A negative bending modulus k_b indicates that inter-

headgroup repulsions are greater than interchain repulsions, favoring bending. A positive k_b indicates that interchain repulsions dominate, which opposes bending. Therefore the third term in **Equation 9** expresses free energy contributions from the vesicle curvature. The first term indicates the attractive contribution, and the second term indicates the contribution from interfacial tension arising from the difference in a compared to a_o. [35].

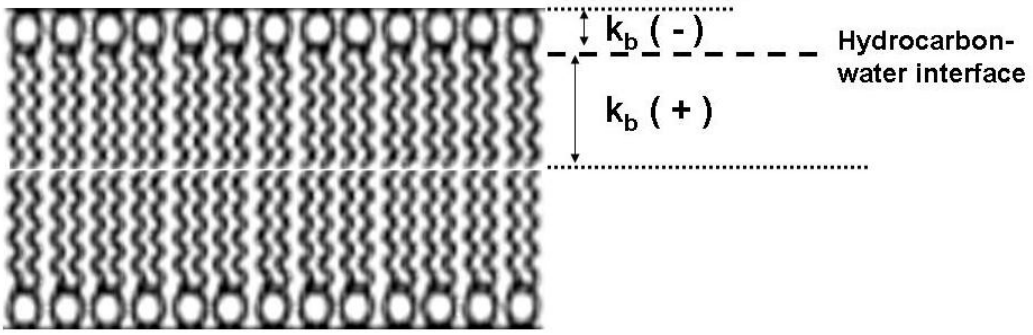

Figure 7. The bending modulus k_b accounts for interheadgroup and interchain repulsions taking place normal to the hydrocarbon-water interface within the bilayer.

When vesicles adsorb to a flat interface, the bilayer curvature ($1/R$) goes to zero. This can cause a large decrease in free energy if the spontaneous curvature of the lipids is in fact zero. **Equation 9** shows that vesicles with $R < R_c$ and $a \neq a_o$ will have greater interaction free energy. Small, highly curved vesicles composed of lipids with zero spontaneous curvature will undergo a greater decrease in free energy upon adsorption onto a flat air-water interface, compared to larger vesicles of the same lipids. Therefore, small vesicles adsorb more quickly to the interface. Vesicles can be reduced in size by sonication [28] or osmotic removal of water [37]. Adsorption can be further facilitated by altering the vesicular lipid composition so that the preferred curvature is closer to zero, thus increasing the energy difference between the curved vesicles and flat monolayer or bilayer.

2.4.2. Molecular geometry determines minimum-energy structure

The critical packing parameter $v/(a_o l_c)$ determines the minimum-energy structure of an aggregate of amphiphiles, where v is the chain volume, l_c is the critical chain length beyond which an extended hydrocarbon chain would not be in the fluid state, and a_o is the optimum headgroup area. **Table 2** summarizes the packing parameter values corresponding to common aggregate structures.

$\frac{v}{a_o l_c} < \frac{1}{3}$	spherical micelles
$\frac{1}{3} < \frac{v}{a_o l_c} < \frac{1}{2}$	non-spherical micelles
$\frac{1}{2} < \frac{v}{a_o l_c} < \frac{1}{1}$	vesicles or bilayers
$\frac{v}{a_o l_c} < 1$	inverted structures

Table 2. Aggregate structures determined by different packing parameters for amphiphilic molecules. Modified from Israelachvili, *Intermolecular and Surface Forces,* 1992.

v and l_c can be calculated from the hydrocarbon chain length as indicated in **Equations 10** and **11**, while a_o is usually measured experimentally and may change with pH and temperature depending on the headgroup.

$$v \approx (27.4 + 26.9n) \times 10^{-3}$$

Equation 10. Volume (in nm^3) of an *n*-carbon chain.

$$l_c \leq l_{\max} \approx 0.154 + 0.1265n$$

Equation 11. Length (in nm) of an *n*-carbon chain.

The number of carbons is given by n, and l_{max} is the maximum extended chain length (in the crystalline state). l_{max} and l_c are in nm. For a molecule with multiple chains, the total v is found by summing the volumes of all chains.

Aggregates with headgroup area $a < a_o$ are energetically unfavored; this geometric consideration yields the critical radius given in **Equation 12**.

$$R_c \approx \frac{l_c}{\left(1 - \frac{v}{a_o l_c}\right)}$$

Equation 12. Optimal radius of a bilayer vesicle.

DPPC has an a_o of 52.3 Å^2/molecule at 25ºC [20]. Each of its 16-carbon chains has a volume of 457.8 Å^3 and a length of 21.78 Å. The critical packing parameter is therefore between 0.5 and 1, indicating that vesicles or flexible bilayers are the minimum-energy structure of DPPC aggregates in aqueous solution.

$$\frac{v}{a_o l_c} = \frac{2(457.8)}{52.3 * 21.78} = 0.804$$

The packing parameter explains the relative reluctance of DPPC to adsorb to the air-water interface, a tendency that can be overcome by mixing DPPC with more cylindrical molecules such as hexadecanol or palmitic acid. These molecules have been shown to decrease the molecular tilt in monolayers of DPPC [38] and DPPC/POPG [39] at the air-water interface. Indeed, the packing parameter of palmitic acid shows that its minimum-energy aggregate structure would be a planar bilayer. Palmitic acid has a monolayer a_o of about 20 Å, and a 16-carbon chain identical to that of hexadecanol.

$$\frac{v}{a_o l_c} = \frac{457.8}{20 * 21.78} = 1.06$$

Exosurf, patented in 1989, utilizes hexadecanol to improve the adsorption of DPPC [40], and tyloxapol. A mixture of DPPC and hexadecanol also functions as a replacement lung surfactant[9]. An alternative synthetic RLS consists of DPPC, cholesterol, and dioleoylphosphatidylethanolamine, which forms inverted structures where the hydrocarbon tails of the lipid molecules face outwards. The composition of this mixture is such that it undergoes a transition from a disordered phase to an inverted phase near mammalian physiological temperature [41]. It was thought that the inverted structures, being hydrophobic, would adsorb to the air-water interface more rapidly than their vesicular counterparts.

2.5.Exosurf

2.5.1. Background and clinical trials

Exosurf (GlaxoSmithKline) is a solution in 0.1 M NaCl of approximately 84% DPPC, 9% HD, 6% TY [40]; that is, 13500 ppm DPPC, 1500 ppm HD, and 1000 ppm TY. It is available for clinical use in the United States as a dry lyophilized powder, stored under vacuum, to be reconstituted with sterile water. Exosurf was intended as a purely synthetic, easy-to-store alternative to naturally-derived surfactants. It is moderately effective in treating NRDS in prematurely born animals [40] and humans [10].

Exosurf is prepared by dissolving powdered DPPC and HD in a solution of tyloxapol and 0.1 M NaCl, gently rotating the sample vials for two hours at 60ºC, dividing into 8-mL aliquots, freezing to -70 degrees Celsius, and removing the water by lyophilization over 24-30 hours to a final pressure of 10 mmHg. Before use, distilled water is added to the resulting powder, which spontaneously disperses, and the contents are drawn into a syringe [40]. This process likely produces large multilamellar vesicles [36].

Early clinical trials of Exosurf in ARDS showed improvements in mortality and lung compliance[42], and oxygenation[43], relative to a saline control. However, the use of Exosurf as an ARDS treatment has been suspended since a 1995 trial with human infants showed no significant improvement over the control [44].

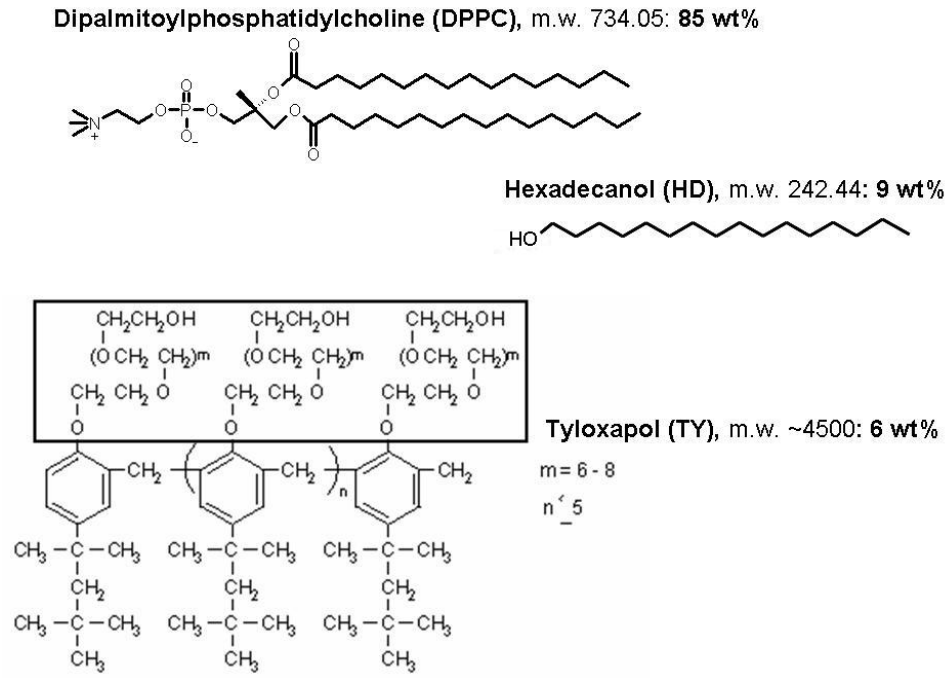

Figure 8. Components of Exosurf, dissolved in 0.1 M NaCl for clinical use. The polyethylene oxide headgroup of Tyloxapol is highlighted. The figure of DPPC is reprinted with permission from Avanti Polar Lipids, Inc. (www.avantilipids.com). The figure of Tyloxapol is reprinted with permission from Sigma-Aldrich Company. (www.sigma-aldrich.com)

2.5.2. Components

The structures of Exosurf's components are shown in **Figure 8.** Dipalmitolyphosphatidylcholine (DPPC) is an essential component in all lung surfactants (LS) for achieving low surface tension, but does not function as an RLS on its own due to its slow adsorption; a 5 mg/mL solution reaches an equilibrium surface tension of 66 mg/mL after 10 seconds adsorption, compared to natural LS [27] .

Hexadecanol (HD) is also intended to maintain low surface tensions and help material to remain at the interface for repeated compression cycles [40]. Mixing HD or PA into a solution of DPPC, spread at the air-water interface, produces a monolayer with a greater area fraction of solid phase at a given surface pressure compared to a monolayer without HD. [38]. This will be explained further in **Section 3.**

Tyloxapol (TY), also sold as Triton WR-1339, can be considered a polymer of the synthetic surfactant Triton X-100, with a maximum of 7 surfactant monomers per molecule and an ethylene oxide chain length of 8-10[45]. TY increases the solution's shelf life and enhances dissolution of the powdered components [40].

TY is also thought to confer a small amount of inhibition resistance. Cheng and Chang demonstrated that adding greater than 10 ppm TY to 1000 ppm DPPC in a pulsating bubble surfactometer reversed the 20 mN/m rise in equilibrium surface tension (γ_e) & minimum surface tension (γ_{min}) caused by 10-100 ppm bovine albumin. However, at lower TY concentrations the surface tension of the solution was closer to that of the albumin solution. High TY concentrations raised the minimum surface tension of the mixture above that of the DPPC-only solution [46].

3. METHODS

3.1.Langmuir trough

3.1.1. History

Agnes Pockels, a self-taught researcher with only a girls' high school education, invented the first Langmuir trough in her kitchen after reading a paper by Lord Rayleigh on finding the molecular area of surface active molecules. She used her device to measure the minimum interfacial area required for an oil film on a water surface. This point became known as the "Pockels point", now called the limiting molecular area. In 1881 she communicated her results to Rayleigh, who facilitated publication of her work in the journal *Nature* [47]. In 1917 Dr. Irving Langmuir used an improved version of her method to determine a Pockels point of 21 Å for fatty acid monolayers on a water surface [48]. His work achieved much wider recognition than Pockels', with the result that the instrument she invented became known as the Langmuir trough.

3.1.2. Measurement of surface pressure

Surface pressure (π) is the force per unit length exerted by the spreading of an amphiphilic molecule on an aqueous surface. This concept can be vividly illustrated by depositing a detergent droplet on a water surface and watching the movement of a paper boat[49] [50] across the surface away from the deposition site. Surface pressure is defined by the relation

$$\pi = \gamma^{o} - \gamma$$

Equation 13. Relationship between surface tension and surface pressure.

where γ^{o} represents the surface tension of the pure subphase, and γ represents the surface tension of the monolayer atop the subphase.

The "improved" film balance utilized by Langmuir [48] measured surface pressure as a horizontally-applied force. The surface pressure was calculated from the smallest weight, attached to a waxed-paper barrier, required to keep the barrier from moving across the water surface with the spreading of the monolayer. The rectangular trough had a surface area of 2-3 square feet. An attached ruler permitted the calculation of the area per molecule.

Modern troughs typically use a Wilhelmy plate to measure surface pressure. The Wilhelmy plate consists of a filter paper or platinum strip, suspended from an electronic microbalance, whose edge is submerged in the liquid. The surface tension and the plate's weight both exert downward forces on the microbalance, while the buoyant force (due to the submerged portion of the plate) exerts an upward force. This can be represented by **Equation 14:**

$$F = (\rho_p lwt)g - (\rho_L hwt)g + 2(w+t)\gamma\cos\varphi$$

Equation 14. Force on a Wilhelmy plate = plate weight – buoyant force + surface tension

where ρ_p is the plate's density, ρ_L is the liquid's density, γ is the surface tension, φ is the contact angle between the liquid and the plate, g is the acceleration due to gravity, and *l, h, w,* and *t* are respectively the length, submerged height, width, and thickness of the plate. The weight and buoyant force contributions are neglected because the initial pressure measurement is set to zero. When the plate is completely wetted by the liquid, the liquid-plate contact angle becomes zero. **Equation 14** therefore reduces to **Equation 15**; the surface tension is calculated from the plate's weight & thickness, and the total force *F* on the microbalance [51]. Surface tension is then converted to surface pressure using **Equation 13**.

$$F = 2(w+t)\gamma$$

Equation 15. Force on a Wilhelmy plate that is completely wet by the liquid, where the pressure sensor is set to zero so that the weight and buoyant force on the plate can be neglected.

3.1.3. Modern trough design

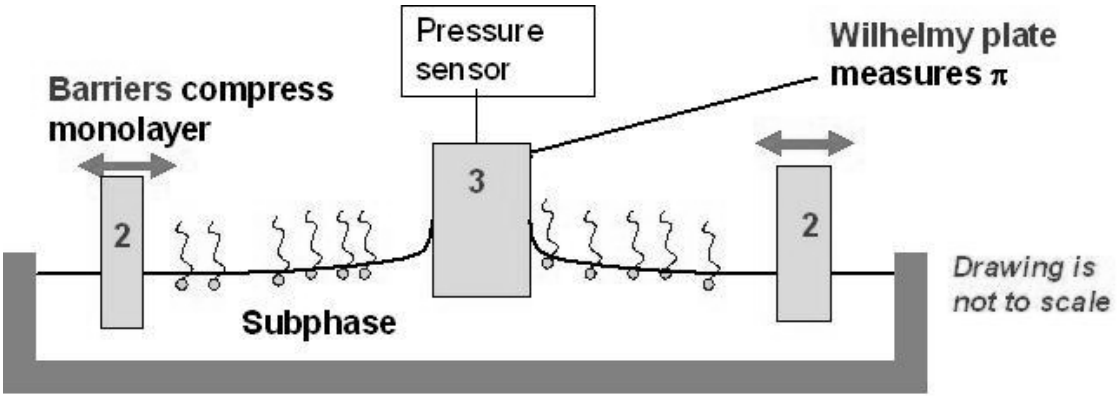

Figure 9. Cartoon of a Langmuir trough with confined area for surfactant (well), barriers and surface tensiometer labeled 1, 2 and 3 respectively.

There are currently several commercially available Langmuir troughs. Manufacturers include NIMA Technologies, Kibron, and KSV. The cartoon in **Figure 9** demonstrates the essential features: (1) a well made of an inert material to hold the surfactant film and water or other subphase (2) a motorized, movable barrier to compress the surface film while permitting the subphase to remain evenly distributed in the well (3) a surface tension measuring device (tensiometer). Not shown is the computer with software and hardware required to control the barrier motors, maintain a fixed trough temperature, and convert the electronic signals of the barrier motors and surface tensiometer into the isotherm exemplified in **Figure 10**. For a single species of surfactant of known molecular weight, or for a surfactant mixture with a calculated number average molecular weight**,** an isotherm indicates the average area occupied per molecule at each surface pressure.

3.1.4. Isotherms: effect of temperature

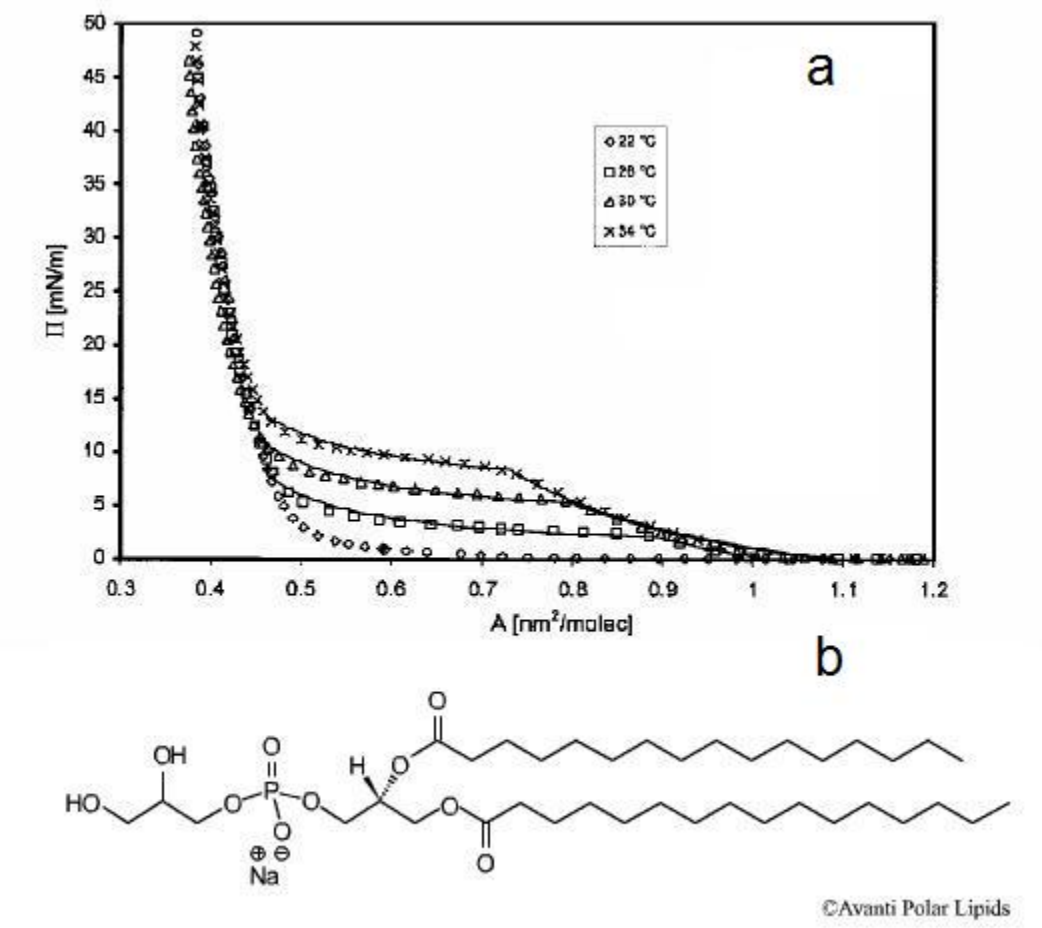

Figure 10. (a) Isotherms of DPPG at different temperatures. X : 34ºC Δ: 30ºC □ : 26ºC ◊ : 22ºC. Reprinted with permission from Vollhardt, *J. Phys. Chem. B.,* 2000. Copyright (2000) American Chemical Society. (b) Structure of DPPG, reprinted with permission from Avanti Polar Lipids, Inc. (www.avantilipids.com)

Pressure-area isotherms, which are plots of surface pressure versus area, are a standard method of characterizing surfactant phase behavior. **Figure 10** shows a pressure-area isotherm for dipalmitoylphosphatidylglycerol (DPPG), a lipid component of LS [52]. As the surface area is reduced, the monolayer undergoes a transition from the low-density gas phase to a higher density fluid phase. This is analogous to the gas-liquid phase transition that occurs when the volume of a three-dimensional gas sample is reduced at constant temperature. Once the sample is

completely in the fluid phase, the pressure rises from zero as the monolayer is further compressed. A sudden change in slope is observed, in **Figure 10** at 10 mN/m pressure for the 34°C sample, as crystallites of a condensed phase begin to form; these crystallites are in equilibrium with the surrounding fluid phase. The transition to nearly vertical slope at high compression forms a completely condensed monolayer. One or more condensed phases may exist, distinguished by differences in molecular tilt angle relative to the surface normal; finally, various solid-crystalline phases may exist, with vertical molecular tilt (*not shown*) [24]. Phase transitions are characterized by changes in the slope of the isotherm; however, an isotherm alone is not sufficient to determine the molecular tilt in a monolayer.

The monolayer exhibits a "critical temperature", T_c , below which the liquid phase does not exist and the monolayer transitions directly from the gaseous to the condensed phase upon compression. This is evident in the disappearance of the gas-fluid transition in isotherms taken below T_c. A limiting molecular area of approximately 0.4 nm^2/molecule, or 40 $Å^2$/molecule, corresponds to the area required for two hydrocarbon chains, which occupy around 20 $Å^2$ each.

The packing profile of the monolayer molecules determines the exact nature of the transitions; for example, a cylindrical molecule may form a highly ordered solid crystalline phase at high compression, while a more irregularly shaped molecule may only form less-ordered condensed phases. DPPG is an example of a molecule that forms a condensed phase rather than a solid crystalline phase; its large headgroup area compared to the area occupied by its hydrocarbon chains prevents it from packing as tightly as a cylindrical molecule such as hexadecanol.

Isotherms are also used to evaluate molecular interactions; for instance, the surface pressure at which a dissolved protein can insert into an established film compared to the pure protein's equilibrium spreading pressure indicates the strength of attraction between a particular surfactant and protein [53].

3.1.5. Isotherms: effect of composition

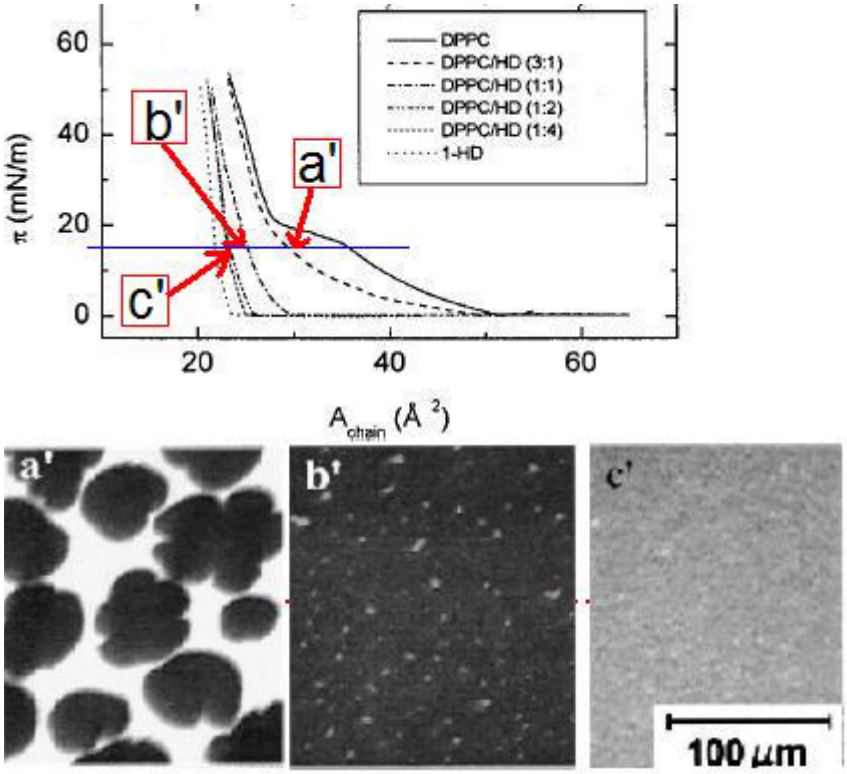

Figure 11. Spread monolayers of DPPC:HD in ratios (a') 3:1, (b') 1:1, and (c') 1:2, plus 0.5 mol% BODIPY FL C_{12} (fluorescent probe). Isotherms were recorded on a water subphase at 30ºC. Images were recorded at surface pressure of 15 mN/m (horizontal dashed line). Reprinted with permission from Lee et al, *J. Chem. Phys.* **2002. Copyright (2002) American Institute of Physics.**

Lee and coworkers [38], using the Langmuir trough in conjunction with fluorescence microscopy, found that addition of cylindrical molecules to monolayers of more conical molecules raises the critical temperature T_c , a characteristic of the monolayer, at which the gas-fluid transition takes place. The effect on the monolayer fluidity at given surface pressure is analogous to lowering the monolayer's temperature.

DPPC was mixed with hexadecanol (HD) in chloroform solution, in DPPC:HD molar ratios of 3:1, 1:1, 1:2, and 1:4. The lipid-analog fluorescent probe BODIPY FL C_{12} (4-4-difluoro-5,7-dimethyl-4-bora-3*a*,4*a*,diaza-*s*-indacene-3-dodecanoic acid) was added at 0.5 mol%; this probe preferentially locates in the fluid phase and is excluded from condensed crystallites, allowing the fluid phase to appear bright and the condensed phases to appear dark in the

fluorescence images. The mixtures were deposited dropwise on a water subphase at 30°C, and the solvent was allowed to evaporate before compression of the monolayer at a rate of 0.1 mm/sec.

The isotherms and images are presented in **Figure 11**, where the x-axis is defined in terms of molecular area per hydrocarbon chain. DPPC contributes two chains, and HD contributes one chain. At 15-16 mN/m, pure DPPC undergoes a first-order phase transition from a fluid phase to a condensed phase, indicated by an abrupt decrease in the isotherm's slope. A second-order transition, from a tilted condensed phase to an untilted condensed phase [54], occurs at 20 mN/m. Mixtures of 1:2 and 1:4 DPPC:HD, and pure HD monolayers, appear to transition directly from the gas phase to the untilted condensed phase, indicating that 30ºC is below the triple point temperature of these mixtures. The addition of HD thus decreased the fluidity of the monolayer, and is equivalent to lowering the monolayer's temperature.

The images a', b' and c' in **Figure 11** provide additional support to this interpretation of the isotherms. Each image was taken at a surface pressure of 15 mN/m. While the bright region representing the fluid phase is abundant in **Figure 11a'** (3:1 DPPC:HD), it is much less visible in **Figure 11b'** (1:1 DPPC:HD) and nearly eliminated in **Figure 11c'** (1:2 DPPC:HD), where the condensed phase now occupies the entire surface area. The DPPC:HD ratio of 3:1 (**Figure 11a'**) corresponds to the composition of Exosurf, which contains DPPC:HD: Tyloxapol in a molar ratio of approximately 75:24:1.

3.2.SAXS

3.2.1. Bragg's law and X-ray diffraction

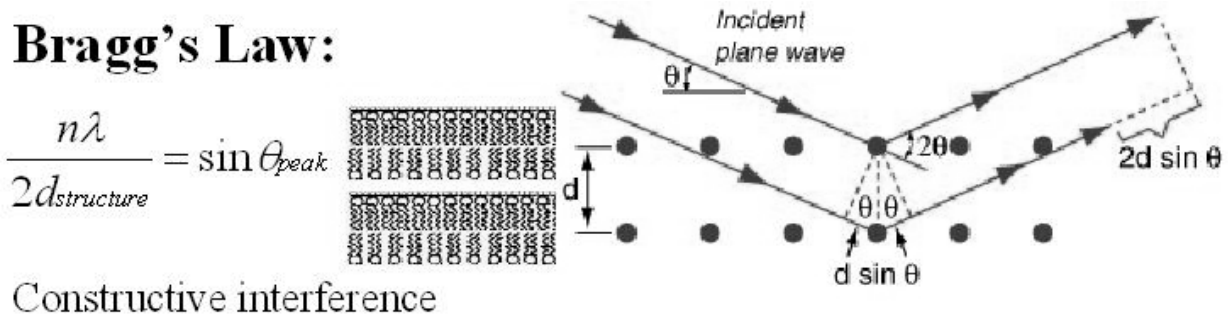

Figure 12. Schematic of diffraction from lipid lamellae.

SAXS is based on Bragg diffraction, where light that scatters from a series of planes exhibits constructive interference at angles (θ_{peak}) that are directly proportional to the light's wavelength (λ) and inversely proportional to the spacing ($d_{structure}$) between the planes (Equation 8). The planes can be oriented so that light is incident from different angles, with each ray's scattering angle equal to its angle of incidence; however, only at the scattering angles satisfying Bragg's law will a diffraction maximum be visible.

$$\frac{n\lambda}{2d_{structure}} = \sin\theta_{peak}$$

Equation 16. Bragg's law.

The scattering vector, q, which is the vector between the incident & scattered beams, is $2\pi/d$ for any distance d. X-ray diffraction data is usually plotted as intensity versus q, and the $d_{structure}$ characteristic of the system is calculated from the q_{peak} at which diffraction maxima are located. Bragg's law can be rewritten in terms of q as shown below. The relationship between the positions of the first-order, second-order and third-order maxima can identify the type of structure. A lamellar structure produces maxima whose positions are integer multiples of the first-order peak position.

$$q_{peak} = \frac{2\pi}{d_{structure}}$$

$$q_{peak} = \frac{4\pi}{\lambda}\sin(\frac{2\theta_{peak}}{2})$$

Equation 17. Relationship between q_{peak}, $d_{structure}$, and θ_{peak}.

The diffraction signal is proportional to source intensity, degree of order, and the difference in electron density between the sample and surrounding medium. In some cases, experimental conditions require the use of synchrotron X-radiation, whose high intensity aids in the characterization of highly disordered or low-contrast samples. Fortunately, the high degree of order in the lipid lamellar system under study allows us to use a lower intensity source, a rotating anode.

Multilamellar vesicles are considered powder samples, which consist of randomly oriented crystallites but are not necessarily dry or "powdery". Each crystallite projects onto the detector a pattern of diffraction spots that is oriented in a slightly different direction than the pattern from other randomly oriented crystallites. These patterns all combine to produce a series of concentric circles with diameter $2\theta_{peak}$. , related to $d_{structure}$ according to Bragg's law (**Equation 16)**, where $2\theta_{peak}$ is in radians. Sample diffraction patterns from lipid lamellae are shown in **Figure 13**.

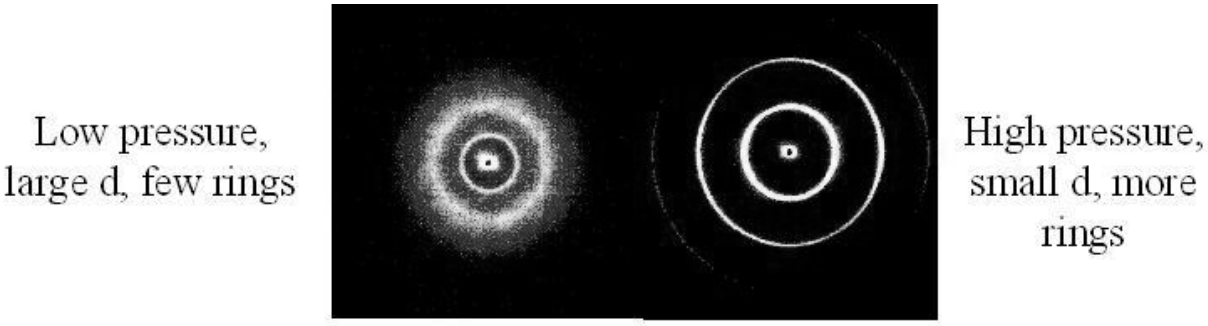

Figure 13. Examples of diffraction patterns from multilamellar lipid vesicles.

3.2.2. SAXS data collection.

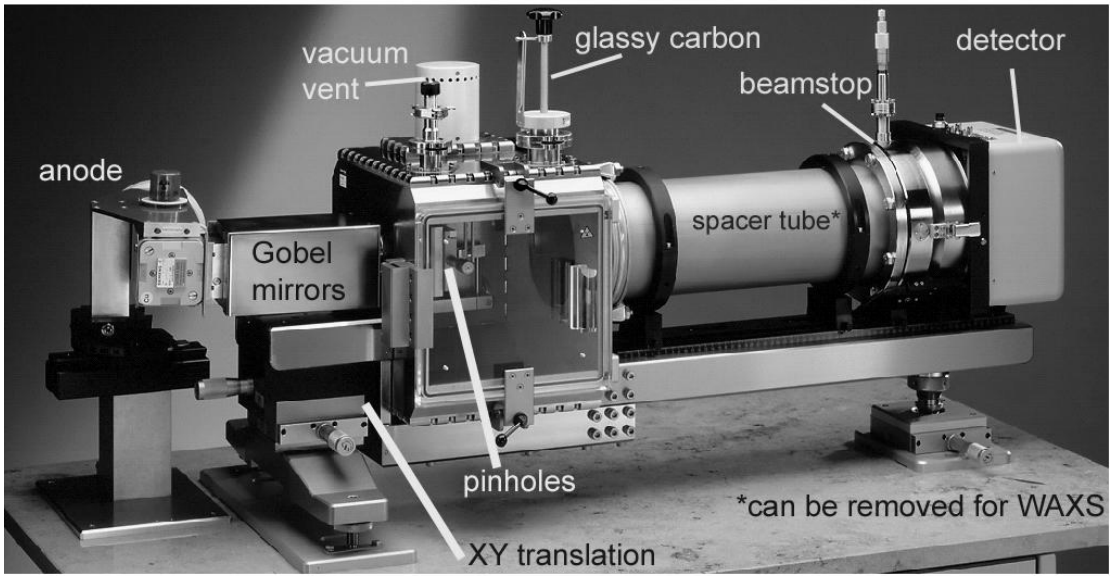

Figure 14. The Bruker Nanostar in SAXS configuration.

The scattering from copper Kα radiation (wavelength 1.54 angstroms) at room temperature under ~ 0.2 torr vacuum was collected from the samples via a Bruker Nanostar small angle x-ray scattering (SAXS) diffractometer, run at 40 kV and 60 mA and mounted on a 6 kW rotating anode.

The Nanostar utilized cross-coupled Gobel mirrors to create a highly parallel beam of copper Kα radiation which was further refined by a .1 mm pinhole approximately 3 inches downstream from the exit aperture of the Gobel mirrors; just before the sample, a .3 mm pinhole trapped scattering created by the .1 mm pinhole. Scattered radiation from the sample and optics was collected by a Bruker HiStar 2D detector placed approximately 65.4 cm downstream from the sample position; just before the detector face, a beamstop approximately 3 mm in diameter absorbed the direct beam. To minimize air-scattering, the entire flightpath between the .1 mm pinhole and the HiStar was held under vacuum in the Nanostar's Anton-Paar Pinhole Chamber.

All samples were loaded and flame-sealed into 1 mm quartz capillaries (Charles Supper Company, Natick, Mass., Cat # 10-QZ). All SAXS experiments were performed at ambient temperature, which varied between 70 and 80 degrees Fahrenheit. Exposure times ranged from 15 minutes to 4 hours.

Intensity of scattering was recorded as average counts/pixel, and background scattering from the quartz capillary was subtracted according to **Equation 19**. The attenuation factor τ_s is obtained with the glassy carbon between the sample and the beam, where "qtz" denotes the empty capillary and "GC" denotes the glassy carbon (**Equation 18**). $I_{total}(2\theta)$ and $I_{qtz}(2\theta)$ are intensity values from the measured diffraction patterns (recorded without the glassy carbon) of the sample capillary and empty capillary, respectively. The attenuation factor expresses how much the sample reduces the beam intensity incident on the quartz capillary walls. Multiplying τ_s by $I_{qtz}(2\theta)$ yields the light intensity scattered from the capillary after passing through the sample. Subtracting this quantity from $I_{total}(2\theta)$ yields the light intensity scattered from the sample alone.

$$\tau_s = \frac{\left(I_{sample+qtz+GC}\right)}{I_{qtz+GC}}$$

Equation 18. Attenuation factor, recorded with glassy carbon.

$$I_{sample}(2\theta) = I_{total}(2\theta) - \tau_s I_{qtz}(2\theta)$$

Equation 19. Background-subtracted sample intensity.

Factors contributing to the scattered intensity include the amount of order in the sample, and the contrast in electron density between the sample and its surroundings. A highly ordered sample produces a stronger scattering signal than a more disordered sample.

See Appendix for further details on SAXS data collection and analysis.

4. EXPERIMENTAL PROTOCOLS

4.1. Materials

All materials were used without further purification unless otherwise indicated.

DPPC: 1,2-dipalmitoyl-sn-glycero-3-phosphocholine was obtained in powder form from Avanti Polar Lipids (Alabaster, AL)

NaCl; Sodium chloride was obtained from Mallinckrodt (Phillipsburg, NJ).

NaAz: Sodium azide was obtained from Alfa Aesar (Ward Hill, MA).

$CHCl_3$: Chloroform was obtained from Fisher.

NBD-PE: N-(7-nitrobenz-2-oxa-1,3-diazol-4-yl)-1,2-dihexadecanoyl –*sn*-glycero-3-phosphoethanolamine, triethylammonium salt was obtained from Molecular Probes, Inc.

DI H_2O: Deionized water (18.2 MΩ-cm, TOC ~ 6 ppb) was used for all aqueous solutions.

Dialysis tubing: 8000 Dalton MWCO, 4mm flat width, regenerated cellulose tubing was obtained from Spectrum Laboratories, Inc. (Rancho Dominguez, CA) and soaked in 0.1 M NaCl for at least 30 minutes before use.

Capillaries: 1 mm diameter quartz capillaries were obtained from the Charles Supper Co.

The following were obtained from Sigma-Aldrich Company:

HD: Hexadecanol

TY: Tyloxapol

PEG10K: Polyethylene glycol, avg. m.w. 10,000

PEG20K: Polyethylene glycol, avg. m.w. 20,000

BSA: Bovine serum albumin

4.2. Exosurf monolayers

4.2.1. Without PEG

The Exosurf and DPPC samples in this study were originally intended for imaging. A fluorescently tagged lipid (NBD-PE) was added to the solution at 0.5 mol% relative to the concentration of DPPC; that is, the solution contained 0.05 moles of NBD-PE for every 99.5 moles of DPPC.

An Exosurf + NBD-PE solution was prepared at a concentration of 1 mg DPPC/mL in $CHCl_3$. 5 mL of this solution contained 4.97 mg DPPC, 0.54 mg HD, 0.36 mg TY, and 0.03 mg NBD-PE. It was stored at -20ºC and protected from light when in use.

A DPPC + NBD-PE solution containing 0.5 mol% NBD-PE in 1 mg/mL total lipids was prepared at a concentration of 1 mg/mL total lipids in $CHCl_3$. 5 mL of this solution contained 4.97 mg DPPC and 0.03 mg NBD-PE. It was stored at -20ºC and protected from light when in use.

The Langmuir trough for these experiments was a KSV Minitrough (KSV Instruments Inc. Finland), whose effective surface area is 18750 mm^2. The trough was equipped with hydrophilic barriers and filled to just below the rim with 160 mL of the subphase solution, which was then brought to 24.5ºC before deposition of the monolayer.

The lipid solutions were thawed by sonication at room temperature and deposited dropwise on the surface. The solvent was allowed to evaporate for 10 minutes before compression of the trough barriers. Surface pressure was measured with a Wilhelmy plate. Unless otherwise indicated, all compressions and expansions occurred at a rate of 7.5 cm^2/minute, and the buffer was pH 7.2-7.4, 150 mM NaCl, 1.5 mM $CaCl_2$, 5 mM tris-HCl.

4.2.2. With PEG

The surface pressure was set to zero at a known volume of PEG-free buffer at 24.5ºC. The buffer was then removed, and the trough was filled with the same volume of 5% PEG10K in buffer. The monolayer was deposited onto the PEG solution and the solvent evaporated for 10 minutes before commencing repeated compressions of the solution.

4.2.3. With bovine serum albumin

An Exosurf monolayer was compressed on buffer at 24.5ºC and held at 50 mN/m while BSA in buffer was injected to a final concentration of 2 mg/mL and gently mixed into the subphase. The barriers were re-expanded at a rate of 7.5 cm^2/minute, and held open for 1.1 hour while BSA adsorbed to equilibrium. The barriers were then re-compressed.

4.3.SAXS sample preparation

4-mL glass vials with Teflon-lined caps were cleaned with detergent, etched with KOH/isopropanol for at least 10 minutes, rinsed with DI H_2O and dried under vacuum while heating.

0.1 M NaCl in DI H2O was prepared, without adjusting pH.

Chloroform stock solutions of 350 mg/mL DPPC, 53 mg/mL HD, and 49 mg/mL TY were prepared. High concentrations were necessary in order to minimize the volume of chloroform to be evaporated.

For a 300-mg sample of Exosurf, in which the total lipid mass (20% of the sample mass) is 60 mg, 147 µL DPPC stock was mixed with 102 µL HD stock and 73.5 µL TY stock. An alternative preparation method consisted of combining larger volumes to make a solution of Exosurf in chloroform, and pipetting a known volume of this solution into each vial.

The chloroform was evaporated by a stream of filtered air blown over the sample as the vial was tilted and slowly rotated to coat the side of the vial with a thin layer of solution. Samples initially appeared clear and colorless, gradually increasing in viscosity and opacity.

The resulting white powdery mixture was stored at 4ºC overnight, resuspended in excess 0.1 M NaCl to a final lipid concentration of 20% by vortexing, and sonication while heating above the melting temperature of hexadecanol (47º-50ºC), using a centrifuge as necessary to collect material at the bottom of the vial. If the vial was not tilted but instead left stationary during the drying process, the layer of dried solid coating the vial was thicker and more difficult to reconstitute.

The control for this experiment was 20% by weight of DPPC in 0.1 M NaCl.

4.3.1. Osmotic stress applied with dialysis membrane

Equilibration solutions containing polymer in 0.1 M NaCl were prepared. The solution compositions are given below by polymer weight percentage in 0.1 M NaCl.

PEG10K: 1%, 2%, 5%, 10%, 20%, 32%, and 40%

The following equilibration solutions were prepared in 0.1 M NaCl plus 0.1% NaAz as a bactericidal agent:

Dextran 150K: 16%, 22%, 31%, 37%

These were added in excess directly to the maximally-hydrated Exosurf or DPPC (approx. 1 mL of PEG10K solution for each 300-mg sample). The samples were then homogenized by vortex, heat and sonication until no visible chunks remained. Samples were stored at 2º- 8ºC for at least 24 hours. To ensure that the system was truly at equilibrium, the solution was changed at least twice. This process consisted of centrifuging the sample to pellet and replacing the supernatant with fresh solution.

4.3.2. Osmotic stress applied with dialysis membrane

Solutions of PEG20K in 0.1 M NaCl, 0.1% NaAz with polymer weight fractions 5%, 20%, 30%, 35%, and 40% were prepared.

The control sample consisted of 10-30 μL Exosurf in excess 0.1M NaCl + 0.1% NaAz, sealed in a 1.0 mm diameter quartz capillary.

Dialysis tubing was soaked in 0.1 M NaCl for 30 minutes prior to use.

Curosurf solutions were prepared in a similar fashion, with 150 mM NaCl + 0.1% NaAz, pH 7.2-7.4 buffer as the hydrating solution.

The 0.1% NaAz was added as a preservative, after it had been determined that NaAz did not change the peak position of Curosurf samples. NaAz was incorporated into the Exosurf samples as follows: Excess 0.1 M NaCl, 0.1% NaAz solution was added to an approximately 300-mg sample of Exosurf + XS 0.1 M NaCl and vortexed to mix. After centrifuging the sample, the supernatant was discarded and replaced with 0.1 M NaCl + 0.1% NaAz.

200-400 μL of the hydrated surfactant were sealed in dialysis tubing and submerged in the PEG20K solutions. Samples were dialyzed for 3-10 days before the PEG20K solution was replaced. Dialysis was continued for an additional three days, after which surfactant was removed and sealed in 1.0 mm diameter quartz capillaries.

4.3.3. Mixing albumin with Exosurf

Solutions of BSA, 100 mg/mL and 1 mg/mL in 0.1 M NaCl, were prepared. Exosurf in 0.1 M NaCl was mixed with BSA to final BSA concentrations of 0.1 mg/mL, 10 mg/mL, and 50 mg/mL using either of the following procedures. The difference in procedure produced no difference in d-spacing.

(1) Repeated cycles of inversion and centrifuge applied to a sealed quartz capillary containing aliquots of Exosurf and BSA in 0.1 M NaCl.

(2) Aspiration of Exosurf solution and then BSA solution into a syringe, without emptying the syringe between solutions, followed by repeated expulsion and intake of the syringe contents in a quartz capillary (pipetting the solution up and down).

4.4.Calculation of osmotic pressure

4.4.1. Range of applied pressures

The BSA solutions exerted pressures of 3.5×10^1 dyne/cm^2 (0.1 mg/mL BSA) and 3.6×10^3 dyne/cm^2 (10 mg/mL BSA). The polymer solutions exerted pressures between 10^5 and 10^7 dynes/cm^2 . Values for the pressure were calculated or obtained from literature as described below.

4.4.2. Osmotic pressure from PEG and Dextran

In order for a solute to exert osmotic stress on a multilamellar aggregate M, there must be a region around M where the concentration of solute molecules is greater or less than their concentration in the bulk [19]. Since this is not the case with NaCl and NaAz, which freely move around M, the PEG or albumin was considered the only osmolyte.

The samples with PEG20K were equilibrated at 4-8ºC and those with PEG10K were equilibrated at room temperature. Rand and coworkers provide data for the osmotic pressure exerted by PEG20K at 7ºC, PEG10K at 30ºC, and Dextran 150K at 20ºC [55]. The following equations fit these data, where P is in dynes/cm^2, and were used to calculate the osmotic stress exerted by specific weight percentages of polymer.

$$\log [P(w_{P10K}, 30ºC)] = 4.99 + 0.29w^{0.60}$$

$$\log[P(w_{P20K}, 7ºC)] = 3.884+1.062w^{0.343}$$

$$\log[P(w_{D150K}, 20ºC)] = 1.385+2.185w^{0.2436} \quad \textbf{for w < 10\%}$$

$$\log[P(w_{D150K}, 20ºC)] = 1.872+1.657w^{0.3048} \quad \textbf{for w > 10\%}$$

Lis [56] derived an expression for the change in DPPC bilayer separation (d_{total}) in response to osmotic stress P (**Equation 20**), where d_{total} in angstroms is equal to the DPPC bilayer thickness (d_{lipid}) plus the thickness of the water layer (d_{water}).

$$d_{total} = d_{lipid} + d_{water}$$

where

d_{lipid} = 44.2 Å at 25ºC in water

$$d_{water} = -2.0 \ln\left(\frac{P}{10^{9.83}}\right)$$

Equation 20. Water spacing between DPPC bilayers decreases with increased pressure.

These data are often plotted with P on the y-axis. Substituting for d_{lipid} and d_{water}, and rearranging **Equation 20**, gives **Equation 21** for osmotic pressure in terms of d-spacing for DPPC.

$$P = 10^{9.83} e^{\left(\frac{d_{total}-44.2}{-2}\right)}$$

Equation 21. Relationship between P and d_{total} for DPPC. From Ref [55].

4.4.3. Osmotic pressure from albumin

The osmotic pressure applied by albumin may be calculated for low concentrations using the van't Hoff law, which is analogous to the ideal gas law.

$$P = [B]RT$$

Equation 22. The van't Hoff law for calculation of osmotic pressure P.

[B] is the molar concentration of a non-dissociating solute, R is the universal gas constant, and T is the temperature in degrees Kelvin. Using this equation, the pressure exerted by 50 mg/mL bovine serum albumin (m.w. approx 69,000 g/mol) can be calculated as follows:

$$\frac{50mg}{mL} * \frac{mol}{69*10^3 g} * \frac{10^3 mL}{L} * \frac{g}{10^3 mg} * \frac{8.314J}{molK} * 298K * \frac{kg*m^2/s^2}{J}$$
$$* \frac{L}{10^3 cm^3} * \frac{10^6 cm^3}{m^3} * \frac{10^3 g}{kg} * \frac{m}{10^2 cm} = 1.8*10^4 \ \frac{g}{cm*s} = 1.8*10^4 \ dyne/cm^2$$

Human serum albumin has a similar molecular weight, and is present at similar concentrations in the blood.

5. RESULTS / DISCUSSION

5.1.Langmuir trough

5.1.1. Isotherms

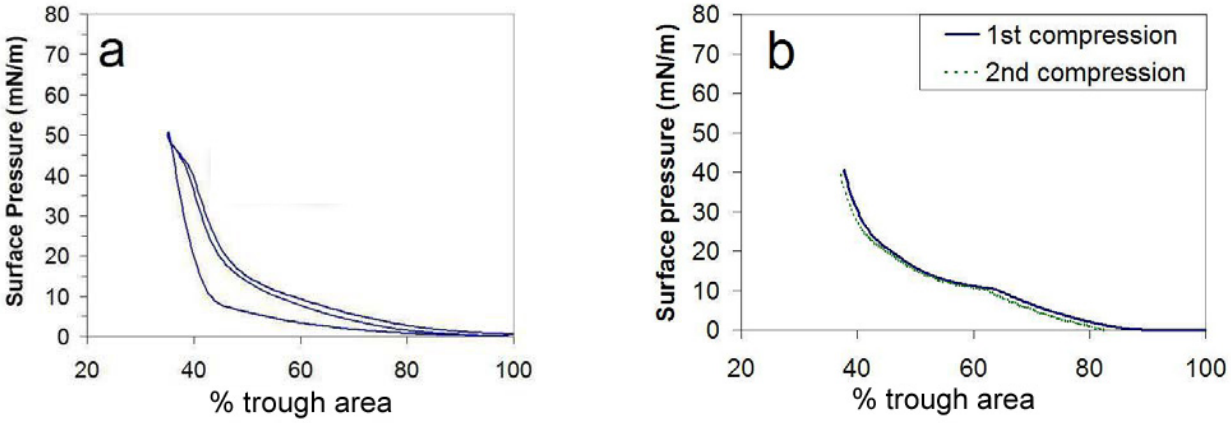

Figure 15. (a) Exosurf + 0.25 mol% NBD-PE (b) DPPC + 0.25 mol% NBD-PE. Samples spread from $CHCl_3$ solution on buffer, and compressed twice in a Langmuir trough at 24.5ºC. Buffer is 150 mM NaCl, 1.5 mM CaCl2, 5 mM tris-HCl, pH 7.25.

The results are presented in terms of trough area percent, since the molecular weight of tyloxapol is not precisely known. This molecular weight is, however, estimated to be 4.5 kDa, or 4500 g/mol [57]. Using this estimate, the average molecular weight of Exosurf is 650 g/mol, with a molar ratio of 75:24:1 DPPC:HD:TY. The molar ratio of DPPC to HD in Exosurf is therefore approximately 3:1, and this isotherm can be compared to the 3:1 DPPC:HD isotherm in **Figure 11.**

The elimination of the fluid-condensed transition seen in pure DPPC (**Figure 15**) at 10 mN/m at 24.5ºC, can be interpreted as a reduction in monolayer fluidity caused by the addition of cylindrical HD molecules, and is consistent with Lee's results [38]. Howver, the phase transition seen in Exosurf at 40 mN/m (**Figure 15**) does not appear in the 3:1 DPPC/HD isotherm, or in the pure DPPC isotherm, of **Figure 11**. In the Exosurf isotherm taken on PEG – containing buffer (**Figure 16**), this transition becomes less prominent upon repeated compression. The transition vanishes from the Exosurf isotherm in **Figure 17** after a single compression and addition of bovine serum albumin (solid blue and dotted red lines).

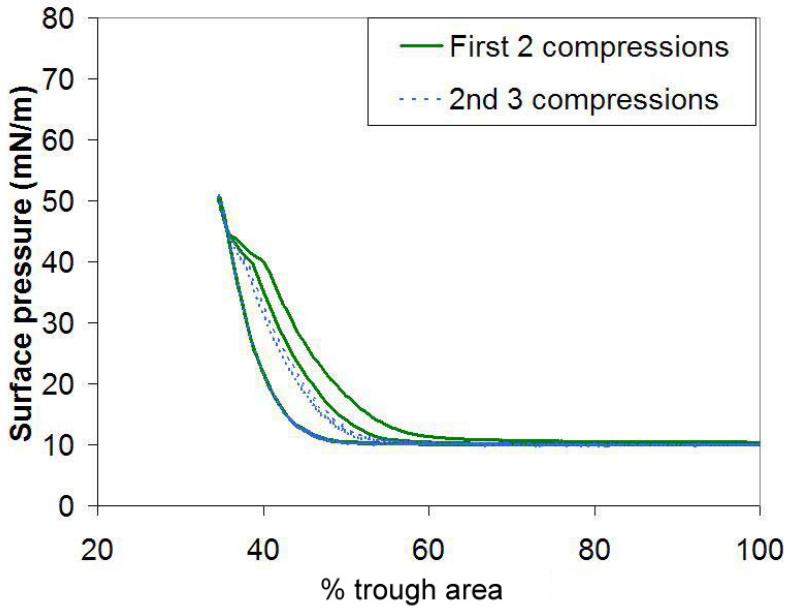

Figure 16. Repeated compressions of Exosurf spread from chloroform on buffer containing 5 wt% PEG 10K at 24.5ºC. Solid line: First two compressions. Dashed line: Second two compressions. Each compression or expansion takes 8.3 min at a compression rate of 7.5 cm^2/ min. Buffer is 150 mM NaCl, 1.5 mM CaCl2, 5 mM tris-HCl, pH 7.25.

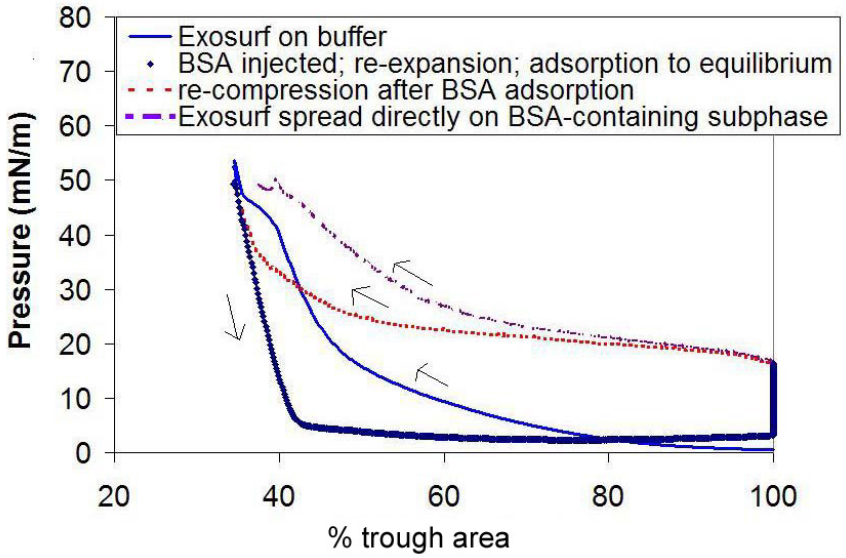

Figure 17. Exosurf + 0.25% NBD-PE compressed on buffer without PEG at 25 C. Bovine serum albumin was injected after compression to a concentration of 2 mg/mL, the barriers were re-expanded, and the albumin was allowed to adsorb. Upon re-compression, the fluid-condensed transition vanishes from the Exosurf isotherm, indicating a change in monolayer composition. Buffer is 150 mM NaCl, 1.5 mM CaCl2, 5 mM tris-HCl, pH 7.25.

A reduction in the slope of an isotherm indicates that surface pressure changes less dramatically with reduction in area. This could indicate the growth of condensed-phase domains in an overall fluid phase, or the collapse of a monolayer component; that is, the formation of surface-associated vesicles, folds, or multilayers that are then lost to the subphase. For example, in **Figure 3** (reproduced here as **Figure 18**), the plateau at 70 mN/m corresponds to the formation of surface-associated material that is visible as bright streaks (**Figure 18B**) in the fluorescence images. The loss of material to the subphase is evident in the hysteresis upon the second compression, which does not typically occur when a monolayer is re-expanded before collapse (compare to the DPPC isotherm in **Figure 15**).

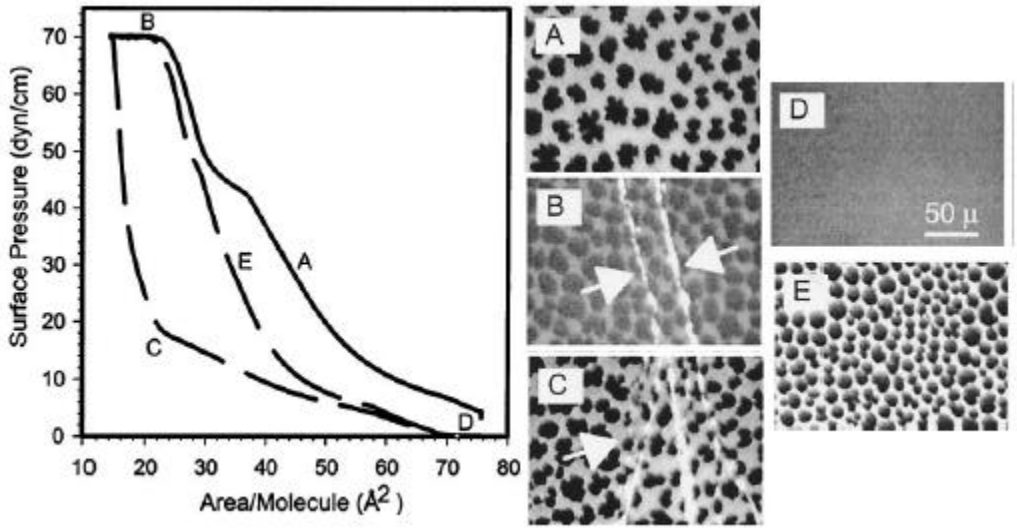

Figure 18. DPPC/POPG/PA 69/21/10 wt% on 25 °C 150 mM NaCl, 2 mM CaCl2, 0.2 mM NaHCO3 , pH 7, 0.5-1 mol% TR-DHPE added for imaging. Images were taken at the surface pressures indicated by the corresponding letters. Bright streaks indicate collapsed material. Reprinted with permission from Warriner et al, *Biophys. J*. 2002. Copyright (2002) Biophysical Society.

Schurch [29] first advanced the argument that Tyloxapol must be squeezed out in order for Exosurf to attain minimum surface tensions. Further consideration of Tyloxapol's solubility in water (**Section 5.1.2**) and the hysteresis evident upon repeated compression of the Exosurf monolayer on 5% PEG10K, indicates that the transition at 40 mN/m in **Figures 15, 16 and 17** may result from the collapse of Tyloxapol and its subsequent loss into the subphase. If this is the case, the rapid removal of the transition on the albumin-containing buffer may depend on the relative concentrations of tyloxapol and albumin. The adsorption of Tyloxapol has been shown to

dominate the surface tension of an albumin-tyloxapol mixture; however, this effect only occurs at high tyloxapol concentrations [46]. In our model of ARDS, the subphase concentration of tyloxapol resulting from its removal at high pressures was not high enough for the collapsed tyloxapol to effectively compete with the adsorption of albumin. In contrast, the isotherm of Exosurf spread directly on an albumin-containing subphase (dotted purple line in **Figure 17**) initially exhibits the surface tension of albumin solution, but at higher compressions it displays a phase transition similar to that observed in Exosurf on albumin-free buffer. In this case, tyloxapol is likely present at the surface in addition to albumin, DPPC, and HD.

Further work is necessary to determine whether the isotherm on PEG-free buffer exhibits similar hysteresis compared to the isotherm on the 5% PEG10K subphase. Faster elimination of the phase transition in the 5% PEG10K case may provide evidence towards a tyloxapol-PEG interaction.

A fluorescence image of the Exosurf monolayer could reveal whether the bulky structure of Tyloxapol disrupts the packing of the DPPC/HD monolayer, allowing it to remain more fluid at given surface pressures. At 15 mN/m the monolayer should display a greater percentage of fluid phase compared to the 3:1 DPPC:HD imaged in **Figure 11a'**.

5.1.2. Tyloxapol solubility supports results

A spread monolayer at constant pressure is gradually depleted by motion between monolayer and subphase, so that at time *t* the trough area *A* may differ from the original surface area A_0 as shown in **Equation 23.**

$$A = A^o e^{-kt}$$

Equation 23. Reduction in trough area over time for a spread monolayer at constant pressure.

This motion can be viewed as diffusion through a thin layer of solution with thickness δ so that the rate constant *k* can be determined by differentiating **Equation 23** and using Fick's law[24], where *n* is the number of moles of amphiphilic molecules. In **Equation 26** defining the rate constant, *D* is the diffusion coefficient and C_f is the equilibrium concentration immediately underneath the monolayer. The bulk concentration *C* is considered to be zero for initial rates of diffusion. Γ is the number of molecules per unit area.

$$\frac{dn}{dt} = AD\frac{dC}{dx} = -\frac{n}{\Gamma}\frac{D}{\delta}\left(C_f - C\right)$$

Equation 24. Fick's law applied to diffusion through a layer of solution with thickness δ.

$$k = \frac{D\left(C_f - C\right)}{\delta\Gamma} = \frac{D}{\delta K}$$

where $K = \frac{\Gamma}{C_f}$

Equation 25. Rate constant for the dissolution of a spread monolayer.

The solubility of stearic acid, a typical monolayer component, is 3 mg/L or 0.003 mg/mL. Tyloxapol is 10^6 times more water-soluble, with a solubility of 100 mg/mL [57], and should therefore dissolve from the interface much faster than the more insoluble DPPC and HD.

5.2. SAXS

5.2.1. Curosurf

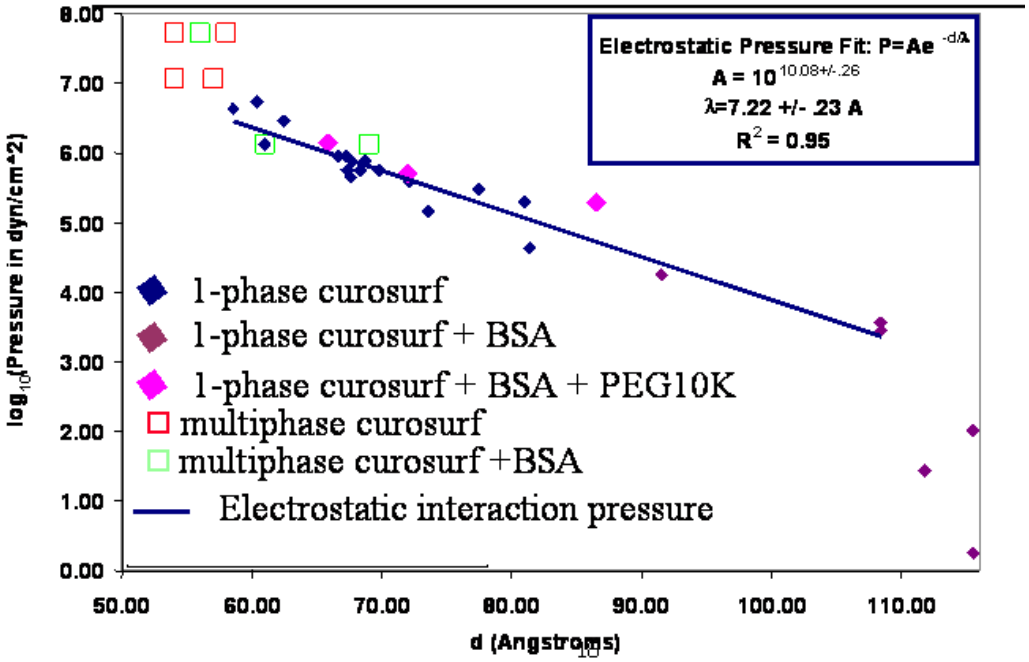

Figure 19. Variation in d-spacing with pressure for Curosurf.

Curosurf experiences a 50 Å change in d-spacing over the range of pressures applied (10^0 to 10^8 dyne/cm^2), with the data falling on the same curve regardless of whether the Curosurf was equilibrated with polymer, albumin or both. The data was fit to an exponential curve with a decay constant of 7.22 ± 0.23 Å. The decay constant is proportional to the slope of the $\log_{10}P$ versus *d* curve. This indicates the nature of the interlamellar interactions, which determine how the system's *d* responds to applied *P*. For example, **Equation 21** for DPPC lamellae in a similar situation has a decay constant of around 1-2 Å. Neutral lamellae whose interactions involve only hydration forces and no electrostatic repulsions are easier to compress, so the $\log_{10}P$ versus *d* curve for DPPC in aqueous solution has a steeper slope. This can be seen in **Figure 20**, where the electrostatic pressure fit for Curosurf is plotted alongside the calculated relationship for DPPC.

The decay constant for Curosurf is close to the Debye length of 7.85 Å in 150 mM NaCl at 25°C, which suggests that there are electrostatic interactions between the lamellae. This is consistent with the composition of Curosurf, which includes a total of 6% negatively charged lipids and 1-2% cationic surfactant proteins. An identical experiment done at 1 M NaCl should yield a decay constant of around 3 Å and would lend further support to this hypothesis.

X-ray reflectivity data [54] shows the protrusion of surfactant protein B (SP-B) about 11-17 Å from the surface of a fatty acid monolayer. This distance, combined with the 43-47 Å estimated thickness of the Curosurf lipid bilayers, produces a minimum spacing of 58 Å that is consistent with the limiting *d* observed in our SAXS data. SP-B may therefore obstruct further compression of the lamellae. SP-B could also be responsible for the single phase to multiphase transition, as areas of the monolayer that did not contain SP-B could be compressed slightly farther than areas of the monolayer with SP-B.

5.2.2. Exosurf

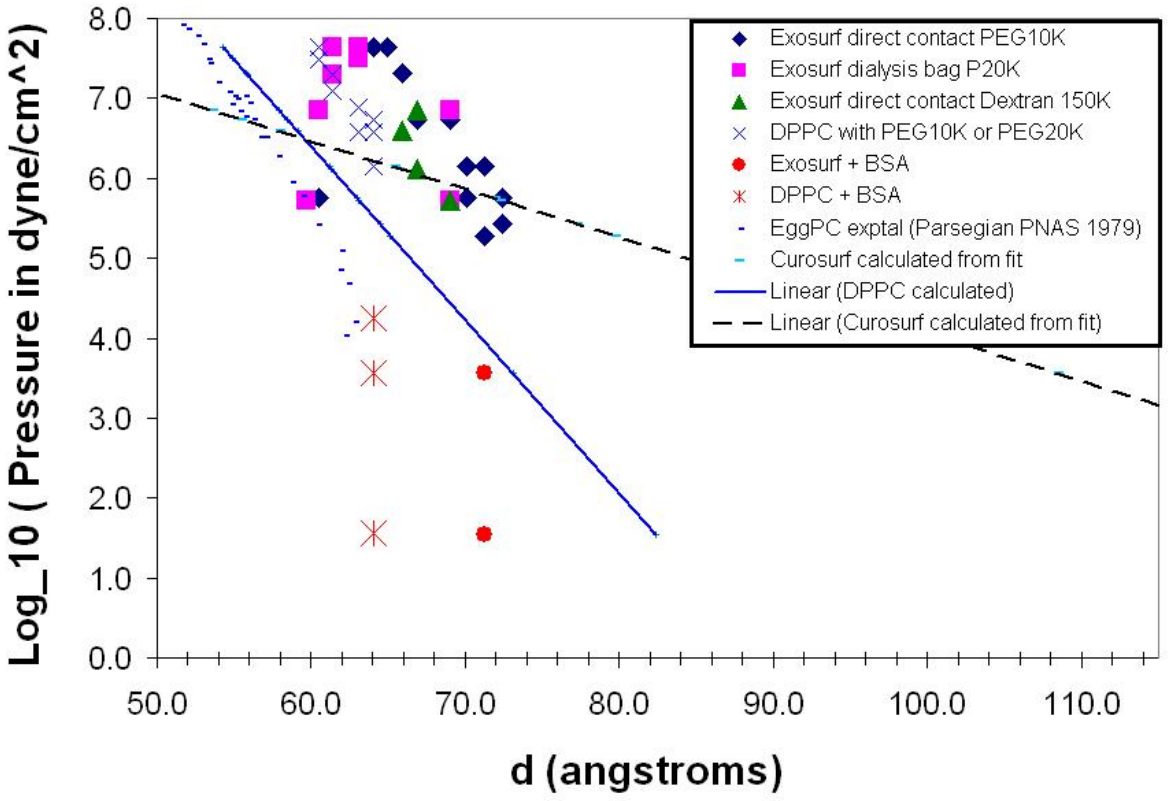

Figure 20. Variation of d with pressure for Exosurf.

Over the range of pressures exerted, Exosurf's d-spacing (**Figure 20**) displays no easily defined trend. In some cases, data points taken at similar pressures have quite different d-spacings. Note the 10 Å difference between the pairs of Exosurf + PEG20K samples at around $10^{5.5}$ and $10^{6.8}$ dyne/cm^2 , and the 12 Å difference between Exosurf + PEG10K samples at around $10^{7.3}$ and $10^{7.6}$ dyne/cm^2 . These differences may indicate separation of the samples into distinct phases with different *d*.

Consideration of Tyloxapol's probable structure in the Exosurf membrane indicates that Tyloxapol may obstruct compression of the lamellae at the pressures applied. Tyloxapol (TY) consists of 7-9 monomers that each contain a 8-10 monomer polyethylene oxide (PEG) headgroup. The thickness (L) of the headgroup layer depends on the configuration of the PEG. Separation of the monomers by a distance greater than $2R_g$ would require them to adopt the

mushroom configuration (spread out along the bilayer surface), while a separation less than $2R_g$ would place them in the brush configuration (vertical and rodlike).[35] The monomer separation in the TY molecule is estimated to be smaller than $2R_g$, since the monomers are linked immediately adjacent to each other; the headgroups should therefore be in the brush configuration. The thickness of a polymer brush layer in a good solvent is given by **Equation 26**, where n is the number of PEG monomers, l is the length of each PEG monomer, and s is the mean distance between polymer molecules (in this case, the distance between adjacent TY monomers) [58].

$$L_{brush} = \frac{nl^{5/3}}{s^{2/3}}$$

Equation 26. Thickness (L) of an adsorbed polymer layer containing *n* monomers each with length *l*, separated by a distance *s*.

Then, given a headgroup length n of 8-10 monomers, an estimated monomer length l of 3.5 Å, and an estimated separation distance s of 3 Å, the thickness of the TY headgroup layer ranges from 31 to 39 Å. Combining this distance with the 43-47 Å thickness of a DPPC bilayer yields a possible d range of 74-86 Å for Exosurf, which is offset by about 14 Å from the 59-72 Å range that was measured. The smaller measured range may be attributed to some entanglement or compression of the TY headgroups that has occurred at the pressures applied. Further investigation at low pressures (10^{-2} to 10^{-1} dyne/cm^2) may reveal the compression of Exosurf lamellae from larger d to the apparent limiting d range observed here. The 10 Å variation in the data may be attributed to differences in the chain length of the PEG headgroups on Tyloxapol.

5.2.3. Conclusions on SAXS data

In order for a solute to exert osmotic stress on a macromolecule (or multilamellar aggregate) *M*, there must be an excess or deficit of solute or water molecules around the macromolecule. If the solute or water distribution is not affected by *M,* then there is no gradient in chemical potential that can dehydrate the space between the membranes. Exclusion of solute from the macromolecule is caused by solute size and the nature of the solute [19]. The observed change in d-spacing with applied pressure on Curosurf vesicles demonstrates that the nonionic polymers are excluded from the lamellae and exert depletion forces. This supports the hypothesis that nonionic polymers dehydrate LS aggregates, and consistent with Tashiro's data showing that polymer improves the surface activity of Curosurf [16].

In the case of Exosurf, the data suggests that protrusion of TY headgroups from Exosurf bilayers obstructs compression of the lamellae over the pressures applied. Another consequence of TY protrusion from Exosurf bilayers is that an aggregate of Exosurf might not experience osmotic stress from added polymer, as the polyethylene oxide groups from the tyloxapol could freely entangle with the polymer in solution and would not form a depletion layer. The lack of definite response to the applied osmotic stress leads us to believe that added polymer at the concentrations that were employed here would not improve the surface activity of Exosurf in the presence or absence of inhibitors.

APPENDICES

I. Protocol for SAXS scans using the Bruker Nanostar

Note: This procedure deals with the use of quartz capillaries; however, alternative sample containers include double sided tape or mica windows.

1. **Load capillaries** (1 mm dia. Quartz).
    a. Place capillary in a test tube padded with Kimwipe. (1/2 kimwipe is usually enough)
    b. Put sample into open funnel-shaped end of capillary
    c. Centrifuge until the sample falls down into the closed end.
        i. This should take <15 minutes at higher centrifuge settings (4-6)
        ii. If the sample is very waxy or thick, it may help to roll the sample into a narrow cylindrical shape prior to placing it in the capillary.
    d. Turn on torch
        i. Open main valve on oxygen tank.
        ii. Open main gas valve near hood
        iii. Open secondary oxygen valve, adjust outlet pressure to < 5 psi.
        iv. Bleed oxygen line & gas line (**check Little Torch Manual for which one to do first)**
        v. Turn on the gas (small red knob) & ignite the flame.
        vi. Turn on the oxygen (small green knob) about 1/8 - ¼ turn. Slowly adjust oxygen & gas till the bright blue cone of flame is at its smallest.
    e. Identify a spot on the capillary that doesn't have sample stuck to the sides. Place this spot in the bright blue flame.
    f. Hold capillary in torch, pulling gently, until it stretches out & seals.
    g. Also seal an empty capillary to use as a background sample.
2. Stick capillaries onto sample holder w/double sided tape.
    a. Razor blades can be used to block out a specific region of the capillary.
3. Setting up SAXS
4. Check the following:
    a. Anode vacuum level : approx 2 x 10^-7 torr.
    b. Chilled water temperature: 17ºC
5. Power up SAXS: gradually increase the kV and mA according to the chart in the manual and/or taped to the SAXS table, approx 2 units every 5-15 minutes. Maximum 40 kV/60 mA.
6. Put sample holder in pinhole chamber (heretofore known as PHK)
    a. loosen the black plastic screws in the chamber to be able to pull back the prongs that fit into the bottom of the sample holder.

b. Make sure the capillaries don't stick too far back towards the wall, otherwise they may hit it & break when you scan in the y-direction.

7. Hit "Reset" button (front panel) so that the "right side door" light turns green.
8. Close vent valve (black cylindrical screw-cap valve, upper left-hand side of PHK).
9. Evacuate chamber to a pressure of approx 10^{-2} torr, by pushing down lever marked "SHUT" on vac pump under SAXS table – **NOT** the vac pump behind the SAXS that is connected to the anode.

10. Create a new project
    a. Under "Project Information" go to Project → New.
    b. Type in a SampleName & SampleNumber. All your scans for this project will have filenames *SampleName_SampleNumber_# # #*.gfrm
        i. example exosurf18_1_000.gfrm
    c. Different runs within the same project can be numbered by changing the SampleNumber when you edit the targets (step 10.c.iii.2)
    d. Put the project in a folder
        i. Type in a path in "Jobname"
            1. example C:\frames\2004\March\March 10\exosurf15
        ii. If the folder doesn't exist you will be prompted to create it

11. Check beamstop position (**usually not necessary**)
    a. Move sample holder so pinhole is not located on a capillary
    b. Collect → Detector → Add , 1-10 s exposure
    c. Should see a dark spot w/ approximately symmetrical corona of brightness around it.
    d. Record exposure time, # counts (intensity)
    e. Calculate counts/sec. Should be ~115; if differs by > 50%, realign beamstop.

12. Check intensity at a given power (**can also do this as part of the Radiography Scan, step 13.b.ii.7)**.
    a. Lower the glassy carbon (faucet-shaped handle on top right-hand side of PHK)
    b. Collect → Detector → Add for 1-10 sec
    c. Record exposure time, # counts
    d. Counts/sec should be ~ 23,000 for 40 kV x 38 mA; ~ 32,000 for 40 kV x 60 mA & PHK vacuum 1.5 x 10^-2 torr

Example counts/sec values at 40 kV/ 60 mA

Intensity (cts/sec)	Pressure in PHK (torr)
25923	5 x 10^-2
42754	8 x 10^-3
32811	1.5 x 10^-2

13. Radiography scan
    a. Lower the glassy carbon
    b. Locate your samples
        i. Collect → Goniometer → Manual
            1. Use handheld controller to move the sample-holder in X-direction (up-down) so that the pinhole is oriented just past the topmost capillary.
            2. Hit Axis Print button on controller; x and y position of that spot should appear on the screen. Record these.
            3. Repeat for lowest capillary.
            4. if the goniometer is not responding to manual control, make sure the "reset" button has been hit
        ii. Collect → Scan → Radiography
            1. enter x and y boundaries of the scan
            2. set 1 second per scan
            3. Do a rough scan of every 0.5 mm in X, 2 mm in Y
            4. A new window will open, color coded by intensity. Mouse over the picture to get the intensity of each point (displayed in lower right-hand corner). Typically lower intensity corresponds to your sample.
                a. If the field looks uniform but you can see that capillaries have been passing in front of the pinhole, check to make sure the "reset" button has been hit & "shutter open" light is displaying.
            5. Once you know where the capillaries are, do a finer scan (0.25 mm in X and Y) to locate the best spots for diffraction pattern.
            6. Make a data table in your notebook:

Sample	Frame	X (mm)	Y (mm)	Intensity_GC (cts/s)	Scan time (s)

("Frame" & "scan time" will be filled in later)

            7. Again, mouse over each spot to find intensity.
            8. Click on them to add them to the "Targets" list, and RECORD THE INTENSITY FOR EACH SPOT because you'll need it for the data analysis.
            9. Also click on one spot in "vacuum" area (not on one of the capillaries) & record its intensity.
            10. Radiography windows can be saved for future reference. They are all automatically named *SampleName*.rad and each new radiography scan will overwrite the other unless you save them under different names.

c. Send targets to program
    i. In the SAXS window (not the radiography window) go to Collect → Scan → Accept Targets and if "Accept Targets" is not checked, click on it.
    ii. In the Radiography window, click Edit → Send targets
    iii. In the SAXS window, Collect → Scan → unclick Accept targets
    iv. In the Saxs window, Collect → Scan → Edit Targets
        1. Change "time" for each scan to 10-60 seconds for the initial run, and longer for the actual data collection
            a. 15 minutes = 900 sec ; 1 hour = 3600 sec
            b. It is sometimes convenient to scan the empty capillary for a shorter amount of time than the sample-containing capillaries. An additional step in the data analysis is required if you do this.
        2. Targets are automatically numbered 1,2,3…; I found it useful to change the SampleNumber so all the targets in the first (short) scan were labeled 1, all the targets in the second (data-collection) scan were labeled 2, and so on.
        3. It may help to copy the whole list into Notepad; the SAXS program deletes all your changes if you accidentally close the Edit Targets window.
        4. This window can also be printed (Ctrl-P).

d. Raise the glassy carbon.

14. Scan → Multitargets
    a. Look at each of your short scans to make sure there is a diffraction pattern.
    b. If there isn't a pattern, either extend the scan time or look at your Radiography window to find a better location, and change that target in the Edit Targets window.
    c. Under "sequence # of ending run" enter the number of scans you wish to take. Example: enter "9" if the frames are numbered 000-008
15. Repeat as necessary
16. During scans: Ctrl-T and arrow keys let you change the display contrast.

II. Extraction of d-spacings using the GADDS software included with the Bruker Nanostar.

A. A quick way to check d-spacing:

1. Analyze→ Cursors → Conic produces a circle-shaped cursor centered on the diffraction pattern.
2. Drag the mouse to expand/contract this circle so it traces one of the rings on the diffraction pattern.
3. On the right-hand corner of the screen the d-spacing corresponding to this ring will appear under "Angstroms."
4. Rings corresponding to a lamellar structure with the same d will be integral multiples of each other. The second ring position will be 2x the first, the third position will be 3x the first, and so on.

B. Integrating the whole pattern:

This process calculates average counts/pixel for each increment of q.

1. Peaks→ Integrate → Chi
2. Chi determines how far around the circle to integrate.
    a. "chi" = 360 degrees goes around the whole pattern.
3. 2-theta determines the radius over which to integrate (i.e. the maximum value of q for which you want to find the average counts/pixel).
    a. "2-theta" = 5 integrates out to the maximum q-value.
    b. At least two rings are needed to determine a structure.
4. Step size determines how large of an increment to step out along the radius.
    a. "step size" = 0.02 is the smallest
5. **Set "normalize intensity" to "1 = Avg counts/pixel"**
6. The region corresponding to the chosen chi & 2-theta will be shown in blue, superimposed on the diffraction pattern.
7. Hit "return" or left-click the mouse to integrate.
8. A plot of I vs. 2-theta will appear superimposed on the diffraction pattern.
9. **Save the file:** A prompt will appear. One of the text fields in this prompt indicates a location where the integrated file should be stored & will say something like "C:\frames\2004…" (the whole text won't fit in the box). Click on the "Browse" button next to this field.
10. A window will appear indicating folders & their contents. Click on folders until you get to where the raw scans are being stored. Example: in C:\frames\2004\Jan\Jan 16 there may be raw scans entitled *SampleName_Samplenumber_xxx*.gfrm.
11. Single-click on one of these scans so its title appears in the text field at the bottom of the box. Change the title to *SampleName_Samplenumber_xxx*_AVGPX.txt (AVGPX indicates that you integrated it by averaging counts/pixel).
12. Create a new folder labeled "integrated data" in the same folder that contains the raw scans, and open this folder so that the newly named file will go into the new folder. Hit "ok" or "open".
13. Repeat B1-12 for all scans, including that of the empty capillary but not including vacuum.

C. Subtracting the background & plotting I vs q.

$I_{sample}(2\theta) = I_{total}(2\theta) - \tau_s * I_{glass}(2\theta)$

$\tau_s = (I_{sample + glass + GC}) / (I_{glass + GC})$, where "glass" denotes the quartz capillary.

The intensity values for calculating τ_s come from the Radiography scan, where you recorded the intensities for each target with the glassy carbon in place. The values for $I_{total}(2\theta)$ and $I_{glass}(2\theta)$ come from the integrated files that you saved in Step B, where $I_{glass}(2\theta)$ is from your scan of the empty capillary and $I_{total}(2\theta)$ is from your sample scan.

SigmaPlot is a quicker & more elegant way to generate the plots but Excel works too.

In Excel:

1. File→ Open → select the file (example: exosurf18_2_000_AVGPX.txt). A preview of the file appears in a gray box.

2. Select "delimited". Scroll down the preview to choose the row at which to start importing, i.e. where the comments end & the data begins. Click "Next"

3. Another box appears. Select "Tab" and "Space" for delimiters.

4. Hit "Next" twice, then hit "Finish"

5. The file will appear as an Excel worksheet titled with the name of the file. The left-hand column shows 2-theta, the middle column shows q, and the right-hand column shows intensity. Paste this into another sheet as necessary for subtraction.

6. Example layout sheet for background subtraction. "c" after filename denotes "corrected" for the background.

				Wt % PEG in equil. Solution		
		EMPTY	**0**	**0**	**5**	**5**
	I_GC(cts/s)	***21824***	***9512***		***15904***	
2-theta	Q	18-2-017	18-2-012	**18-2-012c**	18-2-011	18-2-011c
0	0	3	2	**0.69**	5	**2.81**
0.02	0.001422	5	2.416667	**0.24**	6.166667	**2.52**
0.04	0.002845	5.541667	3.333333	**0.92**	7.333333	**3.29**
0.06	0.004267	32.775	15.75	**1.47**	32.325	**8.44**
0.08	0.00569	106.1731	52.61538	**6.34**	110.4423	**33.07**
0.1	0.007112	218.7344	112.9531	**17.62**	263.5156	**104.12**
0.12	0.008535	234.4306	120.6528	**18.48**	362.2083	**191.37**
0.14	0.009957	135.4783	70.13043	**11.08**	291.8369	**193.11**
0.16	0.01138	76.79	39.55	**6.08**	183.79	**127.83**
0.18	0.012802	48.75893	24.78572	**3.53**	115.1696	**79.64**
0.2	0.014225	33	16.14516	**1.76**	74.52419	**50.48**

In Sigmaplot: set up all the raw data on one side of the sheet, then write transforms to generate the background-subtracted data on the other side of the sheet.

1. Import the data
    a. File → Import: choose your file *SampleName_SampleNumber*_xxx_AVGPX.txt
    b. Choose the row # at which to start the import.
    c. Choose the columns to import
        i. For the first file, import all the columns
        ii. For all subsequent files, import only the 2nd column (intensity)
    d. Select "white space, delimited"
2. Make titles for each column
    a. Format → Col & Row Titles
    b. The columns are, in order: 2θ (radians), blank, Intensity (avg cts/pixel), q (inverse angstroms)
    c. You can keep the 2θ column or paste the q data over it.
    d. Title the "intensity" column with some abbreviation of your sample's name or filename. Example: E1010 is Exosurf + 10% PEG10K
3. Use "transform" function to generate background-subtracted data.

Example:
Quartz capillary in col. 2 has an intensity w/glassy carbon (I_GC) of 21824 cts/s (from Radiography scan) & was scanned for 1800 sec.
sample 18-2-012 has I_GC =9512 cts/s & was scanned for 3600 sec
sample 18-2-011 has I_GC = 15904 cts/s & was scanned for 7200 sec

1	2	3	4	5	6	7
Q	quartz	18-2-012	18-2-011		18-2-012c	18-2-011c
	0	3	2	5		
	0.001422	5	2.416667	6.166667		
	0.002845	5.541667	3.333333	7.333333		
	0.004267	32.775	15.75	32.325		
	0.00569	106.1731	52.61538	110.4423		
	0.007112	218.7344	112.9531	263.5156		

To make the background-subtracted data appear in columns 6 and 7, go to the "Transform" window and write a new transform that is of the form:

$Col(\#) = col(sample)-(time_{sample}/time_{quartz})*col(quartz)*(IGC_{sample}/IGC_{quartz})$

That is,

```
col(6) = col(3)-(3600/1800)*col(2)*(9512/21824)
col(7) = col(4)-(7200/1800)*col(2)*(15904/21824)
```

Then press "Apply". The background-subtracted data should pop up in the appropriate columns. Save this transform window with a new filename, & you can apply it (with minor changes) in other notebooks as well.

BIBLIOGRAPHY

(1) Ueda, T., Ikegami, M. and Jobe, A. **1994**. *Am J Respir Crit Care Med*. 149: 1254

(2) Shier, D., Butler, L. and Lewis, R. **2004**. *Hole's Human Anatomy and Physiology*. USA:McGraw-Hill

(3) Gandy, G., Jacobson, W. and Gairdner, D. **1970**. *Arch Dis Child*. 25: 289

(4) Hudson, L.D., and Steinberg, K.P. **1999**. *Chest*. 116: 74

(5) McHugh, L.G., Milberg, J.A., Whitcomb, M.E., Schoene, R.B., Maunder, R.J., and Hudson, L. D. **1994**. *Am J Respir Crit Care Med.* 150: 90

(6) National Heart and Lung Institute. **1991**. (NIII) 73-432: 165

(7) Boncuk-Dayanliki, P. and Taeusch, H. W. **1995**. *Essential and nonessential constituents of exogenous surfactants.* In: B. Robertson and H. W. Taeusch. *Surfactant Therapy for Lung Disease*. NY: Marcel Dekker, Inc.

(8) Hall. **1992**. *Am. Rev. Respir. Dis.* 145: 24

(9) Clements, J. A. **1982**. Lung surfactant compositions. US Patent #4,312,860

(10) Phibbs, R. H., Ballard, R. A., Clements, J. A., Heilbron, D. C., Phibbs, C. S., Schlueter, M. A., Sniderman, S. H., Tooley, M. D. and Wakeley, A. **1991**. *Pediatrics*. 88: 1

(11) Redenti, E., Peveri, T., Ventura, P. and Zanol, M. **1994**. *Il Farmaco*. 49: 285

(12) Taeusch, H. W. and Keough, K. M. W. **2001**. *Pediatric Pathology and Molecular Medicine*. 20: 519

(13) Taeusch, H. W., Lu, K. W., Goerke, J. and Clements, J. A. **1999**. *American Journal of Respiratory and Critical Care Medicine*. 159: 1391

(14) Kobayashi, T., Ohta, K., Tashiro, K., Nishizuka, K., Chen, W., Ohmura, S. and Yamamoto, K. **1999**. *Journal of Applied Physiology*. 86: 1778

(15) Putz, G., Goerke, J., Taeusch, H. W. and Clements, J. A. **1994**. *J Appl Physiol*. 76: 1425

(16) Tashiro, K., Kobayashi, T. and Robertson, B. **2000**. *Acta Paediatr*. 89: 1439

(17) Parsegian, V. A., Fuller, N. L. and Rand, R. P. **1979**. *Proceedings of the National Academy of Sciences*. 76: 2750

(18) Parsegian, V. A., Rand, R. P., Fuller, N. L. and Rau, D. C. **1987**. *Osmotic stress for the direct measurement of intermolecular forces*. In: L. Packer. *Biomembranes, Part O. Protons and Water: Structure and Translocation*. Boston: Academic Press Inc.

(19) Parsegian, V. A., Rand, R. P. and Rau, D. C. **2000**. *Proceedings of the National Academy of Sciences*. 97: 3987

(20) Lis, L. J., McAlister, M., Fuller, N. L., Rand, R. P. and Parsegian, V. A. **1982**. *Biophysical Journal*. 37: 657

(21) Mishima, K., Satoh, K. and Suzuki, K. **1997**. *Colloids and Surfaces B: Biointerfaces*. 10: 113

(22) Kuhl, T. L., Berman, A. D., Hui, S. W. and Israelachvili, J. N. **1998**. *Macromolecules*. 31: 8250

(23) Kuhl, T. L., Berman, A. D., Hui, S. W. and Israelachvili, J. N. **1998**. *Macromolecules*. 31: 8258

(24) Adamson, A. W. and Gast, A. P. **1997**. *Physical Chemistry of Surfaces*. NY:John Wiley & Sons, Inc.

(25) Gibbs, J. W. **1931**. *The Collected Works of J.W. Gibbs*. New York:Longmans, Green

(26) Chattoraj, D. K. and Birdi, K. S. **1984**. *Adsorption and the Gibbs surface excess*. New York:Plenum Press

(27) Holm, B. A., Venkitaraman, A. R., Enhorning, G. and Notter, R. H. **1990**. *Chem Phys Lipids*. 52: 243

(28) Wen, X. and Franses, E. **2001**. *Langmuir*. 17: 3194

(29) Schurch, S. and Bachofen, H. **1995**. *Biophysical aspects in the design of a therapeutic surfactant*. In: B. Robertson and H. W. Taeusch. *Surfactant Therapy for Lung Disease*. NY: Marcel Dekker Inc.

(30) Schurch, S., Bachofen, H. and Possmayer, F. **2001**. *Comparative Biochemistry and Physiology Part A*. 129: 195

(31) McCormack, F. X. and Mason, R. J. **1995**. *Surfactant therapy for adult respiratory distress syndrome.* In: B. Robertson and H. W. Taeusch. *Surfactant Therapy for Lung Disease*. NY: Marcel Dekker, Inc.

(32) Holm, B. A., Enhorning, G. and Notter, R. H. **1988**. *Chemistry and Physics of Lipids*. 49: 49

(33) Holm, B. A., Wang, Z. and Notter, R. H. **1999**. *Pediatric Research*. 46: 85

(34) Warriner, H. E., Ding, J., Waring, A. J. and Zasadzinski, J. A. **2002**. *Biophysical Journal*. 82: 835

(35) Israelachvili, J. N. **1992**. *Intermolecular and Surface Forces*. London:Academic Press

(36) Szoka and Paphadjopoulous, D. **1980**. *Annual Review of Biophysics and Bioengineering*. 9:

(37) Seitz, M., Ter-Ovanesyan, E., Hausch, M., Park, C. K., Zasadzinski, J. A., Zentel, R. and Israelachvili, J. N. **2000**. *Langmuir*. 16: 6067

(38) Lee, K. Y. C., Gopal, A., von Nahmen, A., Zasadzinski, J. A., Majewski, J., Smith, G. S., Howes, P. B. and Kjaer, K. **2002**. *Journal of Chemical Physics*. 116: 774

(39) Bringezu, F., Ding, J. Q., Brezesinski, G. and Zasadzinski, J. A. **2001**. *Langmuir*. 17: 4641

(40) Clements, J. A. **1989**. Lung surfactant compositions. US Patent #4,826,821

(41) Janoff, A. S. **1997**. Synthetic lung surfactant. US Patent #5,614,216

(42) Weg, J., Reines, H. and Balk, R. **1991**. *Chest*. 1991: 137

(43) Weidemann, H., Baughman, R. and B., d. **1992**. *Am Rev Respir Dis*. 145: A184

(44) Anzueto, A., Baughman, R. and Guntopalli, R. **1995**. *Am J Respir Crit Care Med*. 149: A567

(45) Park, S. Y., Hannemann, R. E. and Franses, E. I. **1999**. *Colloids and Surfaces B: Biointerfaces*. 15: 325

(46) Cheng, C. C. and Chang, C. H. **2000**. *Langmuir*. 16: 437

(47) Pockels, A. **1891**. *Nature*. 43: 437

(48) Langmuir, I. **1917**. *Journal of the American Chemical Society*. 39: 1848

(49) Creative Kids at Home. **2004**. Surface Tension of Water. http://www.creativekidsathome.com/science/water.html. Viewed November 22, 2004

(50) Bloomfield Science Museum. **2004**. Boat Race. http://www.mada.org.il/website/html/eng/6/6-16.htm. Viewed November 22, 2004

(51) NIMA. **1999**. *Tensiometers and Langmuir-Blodgett Troughs: Operating Manual*. NIMA Technology Ltd.

(52) Vollhardt, D., Fainerman, V. B. and Siegel, S. **2000**. *Journal of Physical Chemistry B*. 104: 4115

(53) Brancato, S. and Serfis, A. **2001**. *Journal of Colloid and Interface Science*. 239: 139

(54) Lee, K. Y. C., Majewski, J., Kuhl, T. L., Howes, P. B., Kjaer, K., Lipp, M. M., Waring, A. J., Zasadzinski, J. A. and Smith, G. S. **2001**. *Biophysical Journal*. 81: 572

(55) **2004**. Osmotic Pressure Data. http://aqueous.labs.brocku.ca/osfile.html. Viewed February 13, 2004

(56) Lis, L. J., McAlister, M., Fuller, N. L., Rand, R. P. and Parsegian, V. A. **1981**. *Biophysical Journal*. 37: 657

(57) Sigma-Aldrich. **2004**. Product information: Tyloxapol.

(58) Alexander, S. J. **1977**. *Physique*. 38: 983